Master RADMEP

Master *Radiation and its Effects on MicroElectronics and Photonics Technologies* (RADMEP)

ADVANCED TECHNIQUES IN HYBRID ASSEMBLY OF TUNABLE LASERS: UV-ADHESIVE INTEGRATION AND PACKAGING

Master Thesis Report

Presented by

Hossameldin Elsayed

and defended at

University Jean Monnet

09-09-2024

Academic Supervisor(s): Prof. Sylvain Girard

Host Supervisor (s): Prof. Jukka Viheriälä – Prof. Tapio Niemi

Jury Committee:

Prof. Sylvain Girard – University Jean Monnet

Dr. Arto Javanainen – University of Jyväskylä

Prof. Paul Leroux – KU Leuven

Prof. Frédéric Saigné – University of Montpellier

Erasmus+ UNIVERSITÉ JEAN MONNET SAINT-ÉTIENNE JYVÄSKYLÄN YLIOPISTO UNIVERSITY OF JYVÄSKYLÄ KU LEUVEN UNIVERSITÉ DE MONTPELLIER

ADVANCED TECHNIQUES IN HYBRID ASSEMBLY OF TUNABLE LASERS: UV-ADHESIVE INTEGRATION AND PACKAGING

Abstract

Semiconductor tunable lasers are employed in different applications due to their small size, low cost, and integrability. Their emissions span the spectrum from the visible range (400-700 nm) up to the mid-infrared range (2.5-10 μm). Hence, they are integral to different applications in the fields of communication, sensing, medicine, and spectroscopy. However, realizing high-performance integrated tunable lasers is very challenging. For example, the hybrid integration of different photonic devices usually suffers from misalignment, low coupling efficiency, and long-term instability. In this work, a hybrid integrated tunable laser high performance was demonstrated through UV-curable adhesive assembly. The study presents the usage of UV-curable adhesives and their role in realizing a robust and stable hybrid integration of GaSb-based reflective semiconductor optical amplifiers (RSOA) and Si_3N_4 photonic integrated circuits (PICs). It includes designing a semi-automated assembly process, conducting experiments to characterize the adhesives, and characterizing the hybrid laser. The assembled hybrid tunable laser achieved a maximum output power of 7.7 mW with a current threshold of 117 mA. In addition, wavelength emission at 1984 nm with tuning of 0.1 nm was demonstrated. These findings contribute to the advancement of reliable and efficient hybrid integration techniques for photonic devices.

Keywords: tunable lasers, hybrid integration, UV-curable adhesives, PICs

Preface

My master thesis titled "Advanced Techniques in Hybrid Assembly of Tunable Lasers: UV-Adhesive Integration and Packaging" was completed as my graduation project for the Erasmus-Mundus program "RADMEP". I had the chance to join the Optoelectronics Research Centre (ORC) at Tampere University (TAU) as a research assistant. Since my thesis work was mostly experimental, I had the opportunity to gain hands-on experience at TAU's innovative facilities and cleanrooms. In addition, I managed to be an independent operator of the complicated Micro-Optics assembly machine.

I would like to thank my supervisors at TAU, Professor Jukka Viheriälä, and Professor Tapio Niemi, for their continuous support and guidance through my 6-months internship. I would also like to express my sincere gratitude to Samu-Pekka Ojanen for the great help he offered during the experimental work, and to Aleksander Vlasov for the assembly machine training sessions he gave me, which without I would not be able to complete the project.

I would like to extend my gratitude to my academic supervisor, Professor Sylvain Girard, for following up with me, providing feedback, and making sure I am on the right track to finish the thesis work.

A special thanks to my work colleagues, RADMEP colleagues, and RADMEP coordinators/professors for making lots of good memories during the master's program.

I would like to thank my family for their endless encouragement and support throughout my whole life.

Finally, my deepest appreciation to my favorite, to whom I cannot be more grateful, my lovely wife Johanna, who helped me throughout the whole journey.

Table of Contents

Table of Figures

Table of Tables

1. Introduction

Lasers which can emit coherent light at adjustable wavelengths are integral to different applications in medicine, physics, astronomy, and spectroscopy. The development of semiconductor diode lasers, in particular, has been driven by their compact size, low cost, and high performance. Tunable lasers are one of the most complicated diode lasers available aiming to fulfill the requirement from a widely tunable wavelength range in combination with single mode laser spectrum. Since their first demonstration, tunable lasers have been studied extensively. This thesis focuses on the hybrid integration of tunable semiconductor lasers, leveraging the benefits of both III-V materials and silicon-based devices to achieve efficient integrated tunable laser systems.

The research explores the critical role of UV-curable adhesives in the assembly and packaging of photonic devices. These adhesives offer flexibility, cost efficiency, and ease of processing. However, they require careful selection and optimization to meet the specific needs of different photonic applications. The following sections provide a comprehensive overview of the background and state-of-the-art developments in tunable lasers, highlight the challenges and objectives of the research, and detail the methodology and results of the hybrid assembly process using UV-curable adhesives.

1.1 Background

1.1.1 Tunable Lasers

The first laser diodes were demonstrated in 1962 [1]. In addition, it was observed that their emission spectrum shifts due to alternating their drive current [1] [2]. The organic dye laser is the first broadly tunable laser introduced in 1966 and it was studied for its physical properties and technology [3]. In the early 70s, a proposal for air pollution detection using temperature-tuned diode lasers was introduced. During the same period, a GaAs tunable laser was demonstrated through external cavity tuning [2].

One of the approaches to enhance the applicability of lasers is to achieve a tunable coherent emission. Since its first demonstration in 1966, tunable lasers have been studied extensively as they have a wide range of applications [3]. These studies have led to significant impacts in lots of fields such as physics, medicine, astronomy, and spectroscopy [2][3].

Today, there are many types of tunable lasers, including broadly tunable organic dye lasers, semiconductor lasers, tunable fiber lasers, and free electron lasers [3]. They are also categorized based on their wavelength emission range. Firstly, tunable lasers operating within the visible spectrum (400-700 nm) are used in display technology, fluorescence microscopy, and different spectroscopy techniques [2][3]. Secondly, tunable lasers operating in the near-infrared (NIR) range (700-2500 nm) are utilized in fields such as telecommunications, spectroscopy, and biomedical imaging. Finally, tunable lasers operating in the mid-infrared (MIR) range (2.5-10 μm) are used in gas sensing, environmental monitoring, and medical diagnostics. The MIR wavelengths are highly sensitive to molecular vibrations, making them ideal for detecting a broad spectrum of gases [3]. Thus, tunable laser research is considered to be complementary as each type has a specific wavelength coverage range, power characteristics, tuning speed, size, cost, and other properties [2][3]. Hence, this diversity in tunable laser types has extended the range of its application in different fields.

1.1.2 Tunable Semiconductor Lasers

The two main blocks of a semiconductor laser are a gain chip which has an active medium to amplify a range of wavelengths and an oscillator which limits the oscillation to a narrower range and specific wavelengths [4].

Due to their small size, integrability, low cost, and superior performance, semiconductor tunable lasers have received significant attention as a research topic. The research includes advances in tuning range and speed, device size, and integration techniques [5].

Wavelength tuning is based on the principle of varying the refractive index of the waveguide (WG), which can be achieved through different mechanisms. Firstly, it could be achieved by thermal tuning through either thermo-electric or thermo-optic effect, where temperature variations change the refractive index [6]. Thermal tuning is considered to be the slowest and the most power-consuming mechanism. However, it introduces low to very little losses which is considered as its main advantage [5]. The second mechanism is electro-optical tuning, which uses an electric field to change the refractive index through the electro-optic effect. It is known to be fast and low power consuming. Finally, carrier injection, which is considered to be one of the most commonly used tuning mechanisms due to its high-speed and low-power tuning. However, it suffers from linewidth broadening due to the free carrier absorption [6]. This trade-off between speed, power consumption, tuning range, and noise makes each tuning mechanism suitable for different applications based on their requirements.

To achieve a wide tuning range, micro-ring resonators (MRRs) and distributed Bragg reflectors (DBRs) are commonly used. One of the most commonly used device architectures to realize wide wavelength tuning is tunable external cavity diode lasers (ECDLs) [7]. ECDLs extend the cavity of the laser through external gratings, photonic integrated circuits (PICs) with micro-ring resonators (MRRs), or other optical elements that enhance the tuning range and precision. The mechanism of ECDLs relies on reflecting a portion of the light into the gain chip, thereby creating an extended optical path that can be manipulated for specific tuning requirements [7]. It is advantageous for applications requiring high spectral purity and precision. Finally, integrating lasers that operate in different wavelength ranges can result in a laser array with a broad tuning range [5].

Tunable semiconductor lasers are suitable for a wide range of applications due to their small size, their integration schemes, and the ability to be tuned to different wavelengths. For instance, they are used in dense wavelength division multiplexing (DWDM) as they satisfy the high-speed and capacity communication requirements. For example, 96 channels with a 50 GHz spacing system require a 38 nm wavelength tuning range with linewidth in the order of 100 kHz [5]. In addition, in the field of sensing, tunable semiconductor lasers are used in light detection and ranging (LIDAR) as they provide a wide tuning range for solid-state LIDAR systems which enables large-angle scans. Finally, tunable lasers are used in gas detection as a light source that provides high-resolution absorption spectra to increase the sensitivity of gas detection systems [5].

1.1.3 Hybrid Integrated Tunable Semiconductor Lasers

Since silicon-based optical devices are compatible with the complementary metal-oxide semiconductor (CMOS) fabrication process, they are perfect for realizing passive optical devices. However, silicon is an indirect bandgap material, which makes it very hard to

achieve efficient integrated light sources. On the other hand, III-V materials have a direct bandgap, which gives them excellent light-emitting characteristics. Hence, integrating III-V materials into silicon-based optical devices is an efficient way to realize integrated tunable lasers. The main integration schemes can be divided into hybrid integration, heterogeneous integration, micro-transfer printing, and monolithic integration. The target of all the integration techniques is to make use of different types of gain media and integrate them into available silicon platforms to achieve efficient integrated tunable lasers [5] [8].

One of the most used and mature integration techniques is hybrid integration. Hybrid integration is divided into two main techniques: in-plane butt-joint coupling and flip-chip bonding. The main advantage of hybrid integration is the independence of each device as they can be optimized solely before being integrated. However, the main limitation is that hybrid integration requires high alignment accuracy which makes it difficult to realize industrial mass production. On the other hand, heterogenous integration which is based on direct and indirect bonding schemes seems to be another option for mass production. Although micro-transfer printing and monolithic integration show huge potential, they are not mature and are still in the research and development stage [5].

1.1.4 UV-Curable Adhesives

UV-curable adhesives fall under the category of photocured adhesives which is vital in a wide range of electronic and photonic applications. The definition of an adhesive is a material that can keep two other materials intact and hold together through surface attachment. Mostly, photocured adhesives which are composed of polymers are used in coatings, assembly and packaging, automotive technology, and medical device manufacturing [8].

Being cost-efficient in addition to flexibility and easy processing, polymeric adhesives are increasingly used in different photonic applications [9]. However, as it is considered to be relatively new in the field of photonics assembly, there are some drawbacks and limitations. For example, there is no single adhesive material that can work effectively for all applications. Hence, it is a crucial task to understand adhesive properties to choose the most suitable one for a specific application.

In the context of photonic applications, the characteristics of adhesives that should be considered are viscosity, curing profile, curing shrinkage, transparency, adhesive strength, and operating temperature [9]. Firstly, the resistance of a fluid to flow is defined as viscosity. It is a very important property of photocured adhesives as it describes how controllable the glue dispensing process is going to be. Moreover, viscosity is very temperature-dependent, so the temperature of the assembly environment should be controlled for a consistent and reliable assembly process. Additionally, an adhesive is provided in the soft form of a reactive, cross-linkable monomer blend. In order to convert it from this soft or liquid state to a solid state, the adhesive should be cured. Generally, curing can occur by heat, light, or both. Clearly, from its name, we are concerned with photocured adhesives, the ones that get cured by light. Specifically, the curing profile is the combination of the power of the curing light and the time of exposure. It is a concerning property of photocuring adhesives as it can affect the bonding strength and it can change how uniform the adhesive is cured. Therefore, for each application, the optimal curing profiles are reached through several tests and experiments.

Furthermore, curing shrinkage, which can be divided into volumetric shrinkage and linear shrinkage. Firstly, volumetric shrinkage which quantifies the negative change in

the volume of the adhesive after curing [9]. Secondly, linear shrinkage which quantifies the decrease in one dimension only, usually the distance between the adherends [9]. Curing shrinkage is crucial to study as it can introduce shifts and misalignments between the devices being assembled. Due to their chemical structure, photocured adhesives will suffer from intrinsic losses due to scattering and absorption. Hence, for specific applications, it is needed that the adhesive should have transparency windows in the application region, for example, UV, visible, and near-infrared. Moreover, one of the critical parameters for multi-layer assemblies is high adhesive strength. Thus, the main parameter for assessing the quality of the adhesion is to measure the force needed to break the bonding between the adherends. Additionally, photocured polymeric adhesives degrade under high temperatures. Hence, it is important to define some temperature-related parameters. An important one is the maximum continuous operating temperature, at which the adhesive can stand indefinitely. Another crucial parameter is the glass transition temperature (T_g), which above, the adhesive will lose the hard and rigid properties and transform into a rubber-like soft material.

Packaging of photonic devices and fabricating of planar photonic devices are the two major applications of adhesives in photonics [8]. For instance, in packaging and assembly, fiber optics assemblies are still being developed to make the best out of photocured adhesives. These assemblies' development will help make use of some of the adhesive bonding advantages such as high-speed attachment, protecting devices from the environment, and low cost. However, the main limitation of the assemblies based on adhesive bonding is the misalignment of the devices that happens due to the shrinkage during the curing and polymerization of the adhesive materials. Another limitation of optical device assembly is the failure of full automation. In general, optical alignment requires very high precision and accuracy of less than 1 μm. However, automation can be achieved through a machine semi-assisted alignment to make sure of the quality of the optical devices' alignment [8].

1.2 State of the Art

Recently, significant advancements have been made to realize efficient integrated tunable semiconductor lasers. As in-plane-butt-joint coupling offers direct alignment and integration of different photonic components, it has been the focus of many researchers. However, early attempts faced challenges such as low coupling efficiency and output power. Over time, researchers have made progress in addressing these issues through techniques like passive alignment and the use of specialized WG materials. This section highlights key developments, illustrating the improvements in hybrid assembly techniques.

In 2006, using in-plane butt-joint coupling, Ishizaka and Yamazaki managed to integrate a semiconductor optical amplifier with a photonic integrated circuit (PIC) platform [10] [5]. However, this trial yielded a low coupling output power of 4.7 dBm at 167.5 mA injection current. This was due to the poor coupling between the SOA and the PIC, and between the SOA and the output fiber as well [5]. In 2015, a tunable laser with a 65 nm tuning range and over 100 mW output power was realized by Kobayashi et al [11]. This was achieved via horizontal and vertical passive alignment, and it demonstrated high coupling between different optical chips [11][5]. In 2020, Fan et al. managed to achieve a 70 nm wide spectral coverage and a 3 mW output power with more than 60 dB side mode suppression using a hybrid integrated tunable laser [12]. Finally, due to its high nonlinear threshold compared to silicon, a silicon nitride 800-nm thick waveguide (WG) was integrated to realize a tunable laser with 34 mW output power, more than 70 dB side mode suppression ratio, a tuning range of 58.5 nm, and a 60.7 μs switching time between two lasing wavelengths [13].

In 2023, Ojanen et. al demonstrated a wide tunable semiconductor laser with a tuning range of 170 nm (2474–2644 nm) [14]. This was achieved using a GaSb-based gain chip and a Si_3N_4PIC as a tunable reflector. An average power of 4 mW and a maximum power of 6.4 mW was demonstrated at room temperature. This work targeted the 2-3 μm wavelength range to address the needs for gas sensing applications.

In conclusion, using in-plane butt joint coupling, significant progress, and advancements were achieved in integrated tunable semiconductor lasers. This hybrid integration technique addressed the challenges of low coupling efficiency and output power. Finally, significant research milestones were presented to highlight the ongoing progress and innovation in the field of hybrid integration, facilitating more efficient and robust semiconductor laser technologies.

1.3 Problem Statement

Some challenges remain despite the progress that has been made in integrating various photonic components. Integrating different photonic components may often lead to problems such as misalignment, low coupling efficiency, and inconsistent performance. For instance, challenges such as the precise control of adhesive dispensing, optimizing, curing profiles, and managing curing shrinkage to prevent misalignment are presented when trying to achieve a reliable and repeatable hybrid assembly process using UV-curable adhesives. There is also a need for packaging solutions that would ensure the stability and durability of integrated tunable lasers. Resolving such issues is important for the successful integration and commercialization of tunable lasers in different photonic applications.

1.4 Objectives

The main objective of this thesis was to develop a reliable and repeatable assembly process for hybrid tunable lasers using UV-curable adhesives. The thesis work focused on integrating the GaSb-based reflective semiconductor optical amplifier (RSOA) and the Si_3N_4 PIC designed by Zia and Ojanen [15]. This involved designing the assembly process ensuring that it is compatible with the capabilities and tools of the assembly machine. In addition, the design aimed to tackle problems like heat dissipation and mechanical stability.

Furthermore, the work aimed to optimize the curing and dispensing of UV-curable adhesives. This included studying the relevant properties of the adhesives and selecting the suitable one for the assembly process. In addition, it involved determining the parameters required to dispense specific adhesive volumes and optimizing curing times to prevent underexposure or overexposure.

Finally, after a successful laser assembly, its performance was characterized to validate its functionality. This involved analysing the laser's performance and evaluating it. Subsequently, the hybrid laser is to be packaged in a butterfly package to ensure its long-term stability. This step is critical for transitioning the assembled laser from a laboratory setting to real-world usage, ensuring its robustness.

1.5 Thesis Structure

The thesis is structured in a specific order so that readers can understand the chronological order of the research done. It starts with an introduction to introduce tunable lasers, their applications, and why semiconductor-integrated tunable lasers were extensively studied. It also introduces adhesives, especially photocured ones, their characteristics, and their contribution to different hybrid assemblies. Afterward, some studies that highlight the progress in the field of hybrid integrated tunable lasers were presented. Finally, challenges in hybrid integration were explained before identifying the objectives of this thesis work.

Then methodology is divided into four main sections. The first section gives an introduction to the assembly machine used for this project and its capabilities. Then the second section describes the design process of the assembly. It shows the first design along with its limitations and how the revised design tackles those limitations for a reliable and repeatable process. The third section presents how a reliable gluing assembly process was developed. It starts with a short study on available adhesives and how a specific type was chosen for this assembly project. Afterward, two experiments are presented to characterize the selected adhesive and to optimize its curing profile. It ends with describing the assembly process automation. In addition, all the steps of the assembly process are presented in a flow chart to make it easier to realize how the process is done before presenting the different assembly trials. The fourth and last section of the methodology introduces the characterization and the packaging process of the hybrid tunable laser assembly.

Finally, the results of different assembly trials are presented. Afterward, the performance of the assembled hybrid tunable laser is compared to the performance achieved before assembly. In the end, conclusions of this research project are highlighted before mentioning the relevant future work to be done.

2. Methodology

The methodology section outlines the steps and approaches employed in this study to achieve a successful assembly of the hybrid tunable laser components. By detailing the equipment used, the design processes, and the experiments conducted, this section aims to provide a clear and replicable framework for the methodologies adopted. The subsections that follow will delve into the specific machinery, design considerations, and experimental setups that were integral to this research.

2.1 Micro-Optics Assembly Machine

For the tunable laser assembly, ficonTEC's CustomLine CL1500 [16] for integrated photonics eco-system development at Optoelectronics Research Centre, Tampere University (TAU) was used. It is a multi-purpose micro-assembly machine that has the capability to automate the photonic device alignment and assembly. A system overview is shown in Figure 1 including all the main parts that were used during the assembly process.

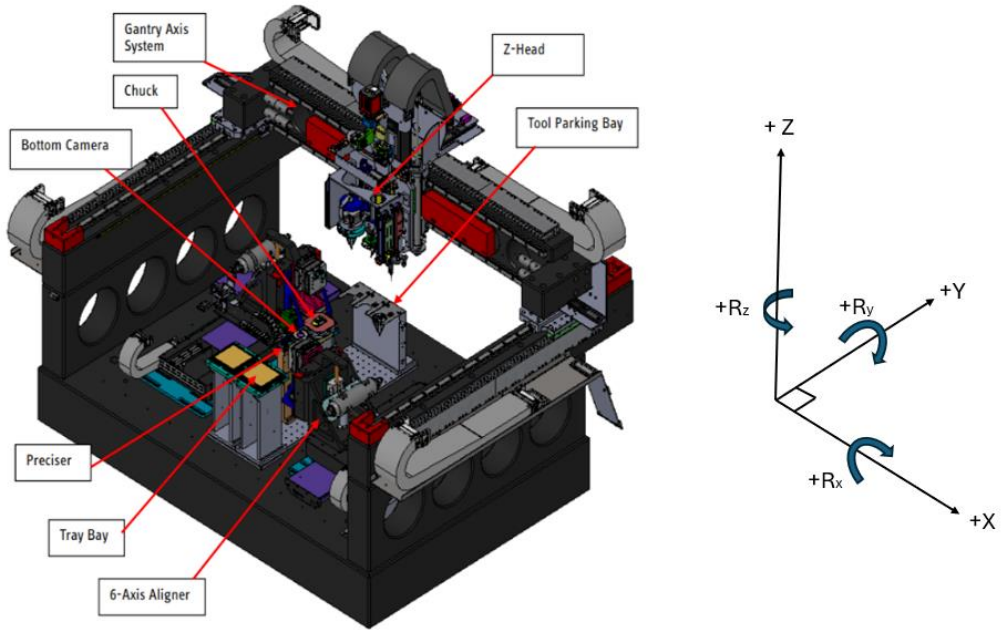

Figure 1: ficonTEC's CL1500 system overview

Firstly, the Z-head is the main moving part of the machine as it has a top camera, adhesive dispenser, and UV-curing LED. It has 6 degrees of freedom so it can be precisely controlled in translation directions X, Y, and Z, in addition to rotational directions Rx, Ry, and Rz through the gantry axis system. Secondly, a 6-axis aligner, where the pickup tool (PUT) can be controlled to grab chips and components using vacuum suction. Thirdly, the bottom camera is used for visualizing components and their orientation. Finally, the preciser, chuck, and tray bay, which can all be used as a station for different components during assembly processes.

Since a UV-adhesive assembly was targeted, information about the adhesive dispenser and the UV-curing LED needed to be known. The UV LED operates at 365 nm and has

a 20-50 mm working distance with an intensity distribution shown in Figure 2. Additionally, the adhesive dispenser is based on a time-pressure-dispensing mechanism.

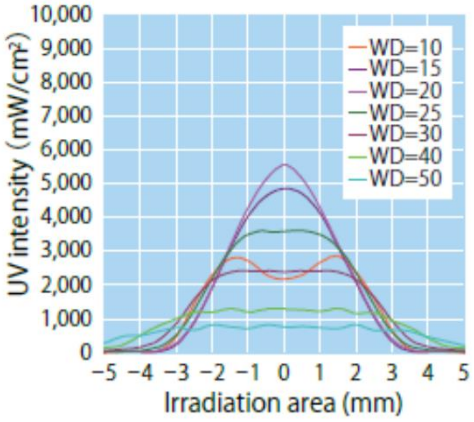

Figure 2: UV LED intensity distribution at different working distances

The machine is controlled by a process control software developed by ficonTEC. The software gives the opportunity to program and develop customized processes. It works in a sequential manner which makes it easier for programming and debugging.

2.2 Designing the Assembly

2.2.1 Initial Design and Challenges

The initial design of the assembly aimed at integrating the GaSb RSOA and the Si_3N_4 PIC as shown in Figure 3.

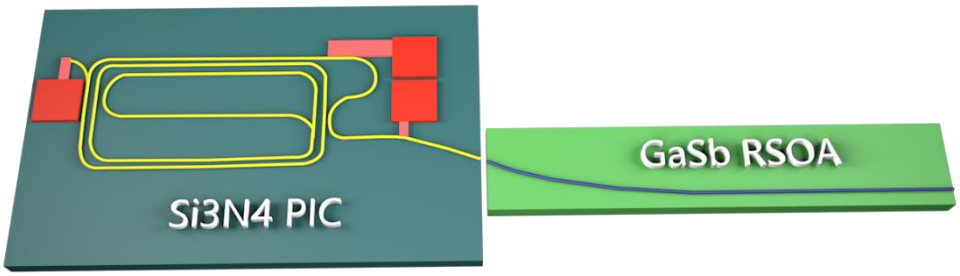

Figure 3: PIC and RSOA - 3D illustration

To ensure heat dissipation and to maintain the components at the same level for a simple and seamless gluing process. The PIC thickness was measured and found to be 0.24 mm, while the RSOA had a thickness of 0.13 mm as shown in Figure 4.

Figure 4: PIC and RSOA thickness – side view

Both chips needed a good heat-conductive base layer for heat dissipation. Hence, as shown in Figure 5, a 0.5 mm thick aluminum nitride (AlN) submount was chosen as a base layer for both chips as it has a high thermal conductivity, which can reach up to 200 W/(m.K).

Figure 5: Assembly design with AlN submounts as heat dissipation platforms

It is noticeable that using the same submount thickness for both chips will make the RSOA side hang with no mechanical support below. Although the adhesive will make both sides attached, the RSOA side will not be able to survive any force applied at its top surface such as the force applied during the wire bonding process. Therefore, the design premise was to reduce the thickness of the PIC's submount so that both sides could have the same thickness as shown in Figure 6. By ensuring that both components have the same thickness, they could be maintained on the same level, making the whole system supported mechanically and simplifying the gluing process as well. To achieve that, silver epoxy was used to bond the RSOA and PIC to their corresponding submount. This epoxy required continuous exposure to a temperature of 170 °C for one minute to ensure a strong bond.

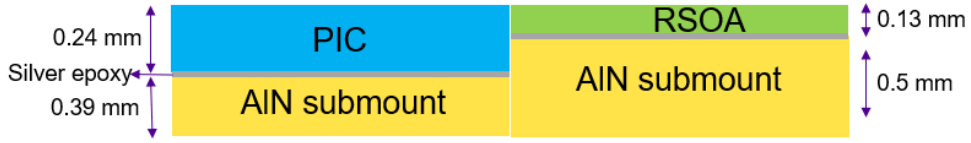

Figure 6: Initial assembly design after thickness matching

The plan for the gluing process involved dispensing two droplets on the side surface of the RSOA's submount as shown in Figure 7. Hence, after alignment between the RSOA and PIC and curing the glue, a strong bond should form between the submounts. The idea of gluing the submounts is beneficial as the number of materials included in the gluing process will be reduced to the minimum where only the CTE (Coefficient of thermal expansion) of the submount and the adhesive need to be matched.

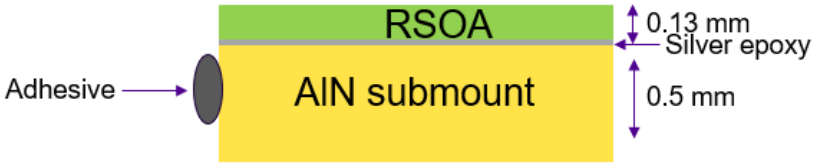

Figure 7: Adhesive dispensing spot on AlN submount side surface

This approach seemed simple and efficient; however, many limitations were identified. Firstly, matching the thickness of both subsystems restricted the ability of the PIC alignment in the z-direction. Secondly, reducing the submount thickness so that both sides have the exact thickness turned out to be impractical. Whether this would be achieved through thinning the submount or ordering submounts with the required thickness, process variations cannot be escaped. Thirdly, the 0.5 mm thick AlN submounts were insufficient as a heat dissipation layer for the hybrid laser. Finally, dispensing adhesive droplets on the side of the submount using a straight tip was impractical and challenging. The straight tip had the chance to hit the facet of the RSOA before reaching the dispensing spot on the side surface of the submount. The limitations of the first design are illustrated in Figures 8, 9, 10, and 11.

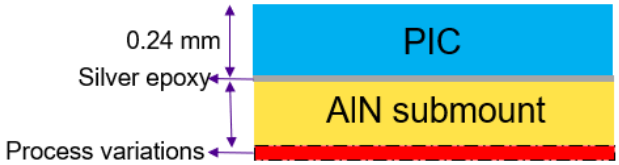

Figure 8: Process variations affecting the desired thickness of the AlN submount

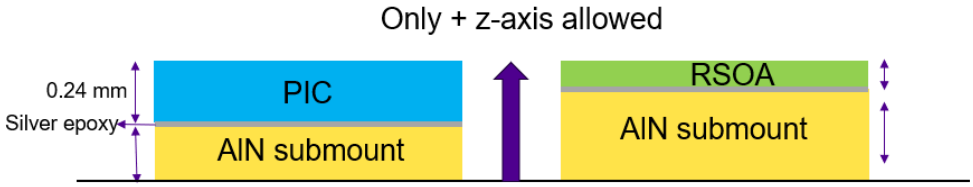

Figure 9: Thickness matching limiting moving in the negative z-axis direction

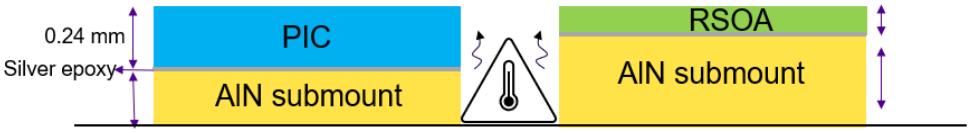

Figure 10: Insufficient heat dissipation from both submounts

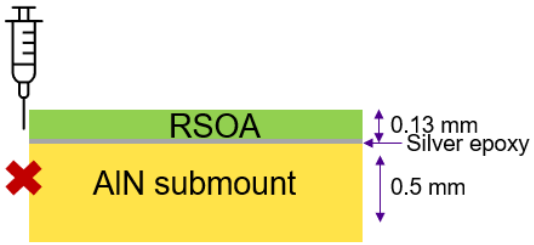

Figure 11: Straight syringe tips with limited reach for the AlN submount below the RSOA

2.2.2 Revised Design

Based on the limitations found in the initial design, several adjustments were made to make the assembly process more efficient. The new design eliminated the need for matching the thickness of the PIC and RSOA subsystems. The RSOA and the PIC were mounted on the 0.5 mm submounts without undergoing any thinning process. This change made the assembly process more flexible and practical.

To tackle the heat dissipation problem and facilitate the assembly process, an aluminum part with a step was designed as a base for the assembly process. As shown in Figure 12, the RSOA on its submount was placed and bonded on the higher step of the aluminum platform using silver epoxy, while the PIC with its submount was placed on the lower step to allow better vertical movement for active alignment before gluing. Having a high thermal conductivity, aluminum, seemed to be a proper heat dissipation platform.

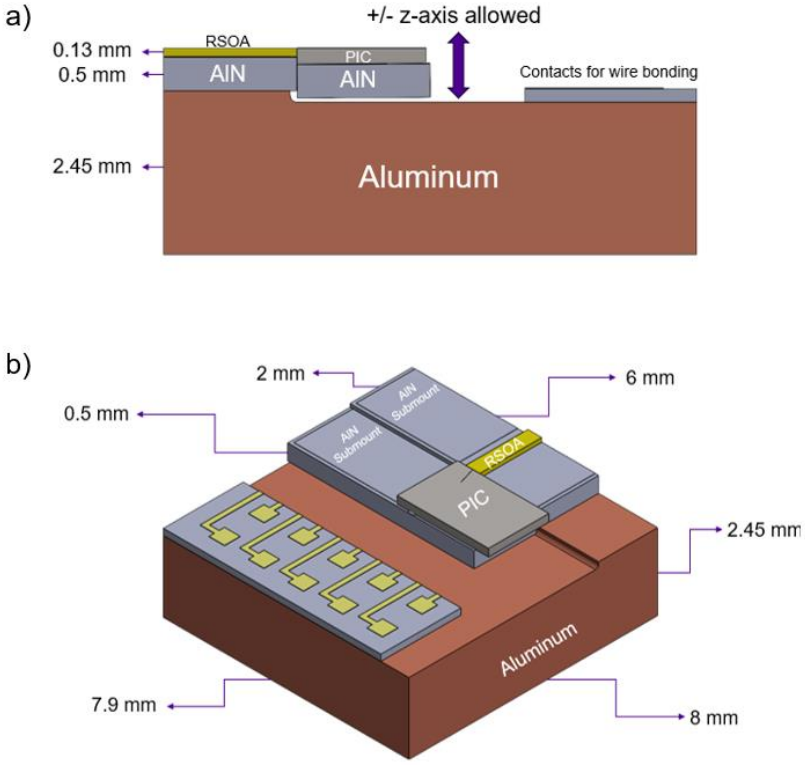

Figure 12: Revised design schematic - a) side view. b) isometric view.

These dimensions were selected so that the laser system fits in the chosen butterfly package as shown in Figure 13.

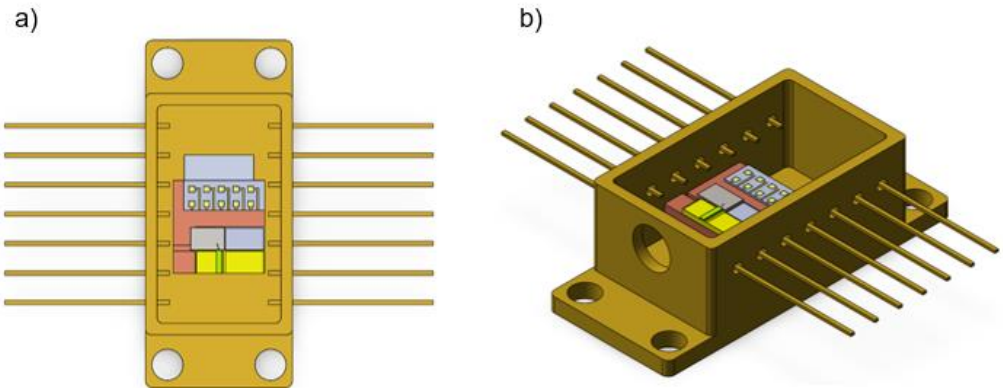

Figure 13: Schematic of packaged assembly - a) top view. b) isometric view.

In addition, the thickness of each layer was designed to make the emitted light at the center of the package outlet as shown in Figure 14.

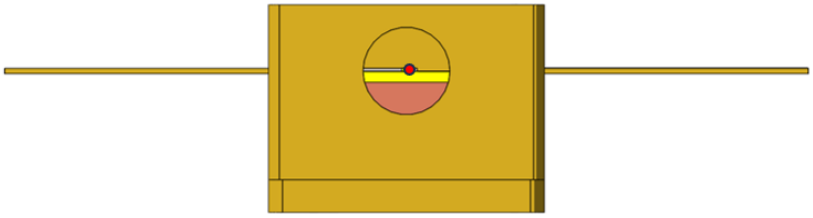

Figure 14: Laser output at the center of the circular aperture of the butterfly package

Additionally, a 90-degree bent tip was ordered to overcome the adhesive dispensing challenge. The bent tip seemed to be a perfect tool for dispensing adhesives on the side surfaces of the AlN submounts. This ensured a more practical and reliable gluing process, overcoming the constraints of the initial design.

The main challenge of this design is the gap between the PIC subsystem and the lower step of the aluminum part. As shown in Figure 15, this gap is designed to be 60 µm. However, due to process variation which could be ±50 µm, the gap would be between 10-110 µm. Firstly, this gap needed to be filled with a thermal conductive material to use the aluminum part as an efficient heat dissipation platform. Secondly, if not filled, it will make the PIC subsystem not mechanically supported and it might not handle the wire bonding required for packaging. To solve this problem, experiments will be done using silver epoxy to fill this gap after the glue assembly of both the RSOA and the PIC.

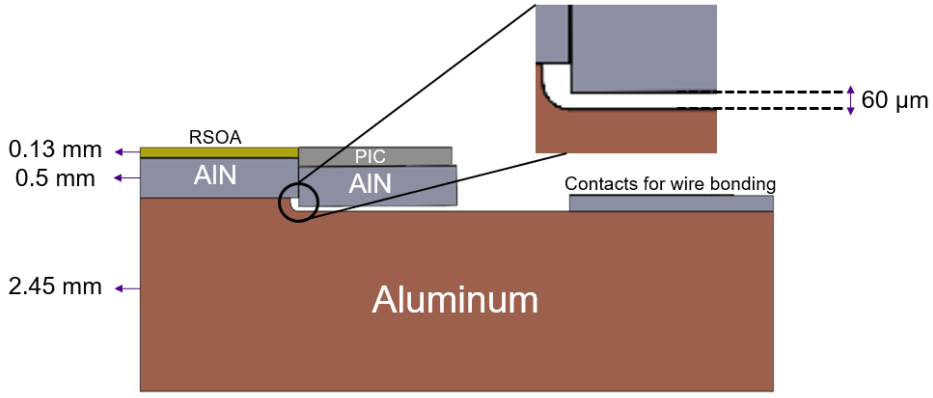

Figure 15: The gap between the PIC subsystem and the lower step of the aluminum part as main challenge for the assembly design

In conclusion, the revised design addressed the main limitations identified in the initial design. It was achieved by adding a better heat dissipation platform, allowing for better active alignment, and improving the adhesive dispensing process. A reliable and efficient hybrid assembly of the tunable laser components was aimed through this modified design.

2.3 Developing a Reliable Gluing Assembly Process

To achieve a reliable and strong bonding between chips, optimizing the UV-gluing process was necessary. Since optimizing all the parameters of the process would have been time-consuming, only two parameters were the main concern of this optimization process. The first one is the adhesive droplet dispensed volume, as a percentage of it will represent the volume shrinkage happening during the process. The second one is the curing time profile to ensure that the glue is neither underexposed nor overexposed.

From a wide range of curing adhesives, DB-OB786 was selected for the assembly process. Hence, the glue experiments were done using this adhesive to control the volume of dispensed droplets and to reach the optimum curing profile.

2.3.1 Selection of UV-Adhesives

As explained in the introduction, the main challenge of using adhesives is that there is no one type that is optimum for all kinds of applications and assemblies. Hence, choosing the right adhesive for the assembly process was a crucial task. The main characteristics that were of concern for the assembly process include viscosity, curing profile, curing shrinkage, bond strength, coefficient of thermal expansion, and operating temperature.

An initial comparison was conducted between four good candidates based on their availability at TAU. Table 1 shows the adhesives available along with their relevant characteristics.

Table 1: Comparison between different properties of available adhesives

Adhesive commercial name	Viscosity	Shrinkage	T_g	CTE
Optocast 3410 [17]	90,000-140,000 mPa.s	~0.07 %	150℃	14 ppm/℃
DB-OB786 [18]	32000 mPa.s	~1.6 %	179℃	38–53 ppm/℃
Vitralit 1860 [19]	35000–50000 mPa.s	~1.5 %	100–120℃	90–120 ppm/℃
NOA61 [20]	400 mPa.s	~1.5 %	100–120℃	-

Based on this brief comparison, Optocast 3410 seemed to be the best adhesive as it has the highest viscosity, lowest shrinkage, lowest CTE, and high T_g. However, it was unfortunate to find that the available stock of this adhesive was expired and not functioning properly. Based on the internship duration and due to a lead time of 2 months to purchase a new and functional Optocast adhesive, it was decided to work with the available adhesives. Although NOA61 has a low shrinkage, its low viscosity made it unsuitable for the process as the dispensed droplets would not stay on the side surface of the submounts. So, the final choice was between DB-OB786 and Vitralit 1860. Their characteristics are good and suitable for the process, however, DB-OB786 has the advantage of higher T_g and lower CTE. Hence, DB-OB786 was chosen for the assembly process of the hybrid tunable laser.

In selecting DB-OB786 as the adhesive for this project, all the relevant characteristics were evaluated as follows [18]:

Viscosity: The resistance of a fluid to flow is defined as viscosity. It is a crucial property of photocured adhesives as it influences the control of the glue dispensing process. DB-OB786 has a viscosity of 32000 mPa·s, making it suitable for precise and controllable dispensing, essential for accurate photonic assembly.

Curing Profile: The curing profile, which combines the power of the curing light and the time of exposure, affects the bonding strength and uniformity of the cured adhesive. According to the datasheet, DB-OB786 requires a typical light fixation time of 3-10 seconds with a 365 nm LED at an intensity of 1000 mW/cm². These curing conditions can be achieved through the curing LED of the assembly machine. Hence, the curing profile could be optimized through the designed experiment.

Curing Shrinkage: Curing shrinkage quantifies the volume reduction of the adhesive post-curing, which can lead to misalignments in assembled devices. DB-OB786 has low shrinkage, with a reported value of 1.6 vol. %, minimizing the risk of misalignment and ensuring stability in the assembled components.

Bond Strength: High bond strength is crucial for multi-layer assemblies. DB-OB786 demonstrates excellent adhesive strength, with compression shear strength values ranging from 20 MPa (glass) to 41 MPa (anodized aluminum). This high strength ensures robust and durable bonds between the adherends.

Operating Temperature: Photocured polymeric adhesives degrade under high temperatures. DB-OB786 is suitable for use between -40 to 180 °C and has a high glass transition temperature (Tg) of 179 °C, which ensures it maintains its properties and stability even in high-temperature environments.

Standards: The adhesive is free of solvents, has low outgassing, and low swelling, and is reproducible, making it reliable for high-precision applications. It also complies with RoHS Directive 2015/863/EU and is halogen-free according to IEC 61249-2-21, ensuring it meets environmental and safety standards.

These properties make DB-OB786 an ideal choice for photonic device packaging and assembly, where precision, reliability, and durability are required. Therefore, it was the chosen adhesive for the hybrid tunable laser assembly.

2.3.2 Experiment 1: Dispensing Parameters

The ficonTEC machine includes a time-pressure mechanism for dispensing adhesives. This mechanism is based on applying a specific pressure on the adhesive syringe for a period of time to dispense a specific amount of the adhesive used. To control the volume of the dispensed adhesive, this experiment was designed. The two main objectives of this experiment are, firstly, to quantify the effect of pressure application time on the average volume of dispensed curing adhesive droplets. Secondly, to determine the uniformity of dispensed droplet volumes under varying pressure application times. To address these objectives, the experimental variables were defined and controlled as follows:

Experimental Variables

Independent Variables:

- Pressure application time (150 ms- 600 ms with a step of 50 ms)

Dependent Variables:

- Volume of dispensed adhesive droplets

Controlled Variables:

- Substrate type: Silicon
- Pressure: 0.5 bar
- Dispensing syringe
- Adhesive type: DB-OB786
- Syringe tip diameter: 0.41 mm
- Number of droplets per batch: 10

- Environmental conditions: Temperature and humidity
- Measurement technique for droplet volume
- Distance between tip and sample: 250 μm

Experimental procedure

Firstly, the silicon substrate was cleansed with isopropanol to make sure that big-size (more than 1 mm^3) contaminants were removed. Then, a 0.41 mm-diameter tip was applied to the adhesive syringe before being installed in the assembly machine.

The experiment was divided into ten batches, each corresponding to a different pressure application time. For each batch, 10 droplets were dispensed on the substrate at a specific pressure application time. The distance between the dispensing tip and the substrate surface was fixed to be 250 μm to ensure uniformity of droplet shape. In addition, the distance between dispensed droplets is fixed at 3 mm in all directions. This experiment was done at one of TAU's cleanrooms. Hence, temperature and humidity were controlled outside and inside the assembly machine to minimize external variations.

After each droplet is dispensed on the substrate, its diameter and height are measured through the vision system of the assembly machine. Although this approach took much more time than if all droplets were to be dispensed first and then all to be measured at once, it was decided to do the immediate measurement of each droplet to avoid losing the hemisphere shape of the droplet. Taking measurements while the droplet is keeping its hemisphere shape is important as the volume is calculated based on the approximation that the droplet is initially a hemisphere. The volume approximation is shown in Figure 16 along with equation (1) to calculate the volume of each droplet.

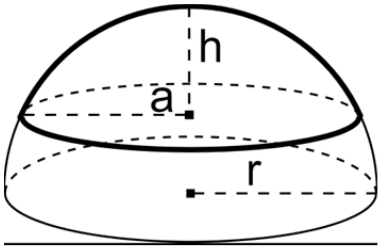

Figure 16: Adhesive droplet volume approximation as a hemisphere

$$\text{Volume} = (1/6) \times \pi \times h \times (3a^2 + h^2) \qquad (1)$$

Finally, after the measurements of all the droplets are recorded, the average volume for each batch is calculated and plotted against the corresponding pressure application time.

Note: Typical times for various experimental steps are as follows: substrate and adhesive preparation—1-2 hours, dispensing and characterizing 100 droplets —3 hours,

and data analysis—1-2 hours. It is also worth noting that 8 trials with a low number of droplets were needed to automate the whole process before doing the full experiment.

Results and Discussion

After dispensing 10 batches with 10 droplets per batch as shown in Figure 17, a total of 100 droplets were dispensed on the silicon substrate. The data were collected, analyzed, and plotted in Figure 18 to understand the relationship between pressure application time and dispensed droplet volume. The graph also included error bars representing the minimum and maximum volumes away from the fitted line to illustrate the uniformity of the droplet sizes at each pressure application time.

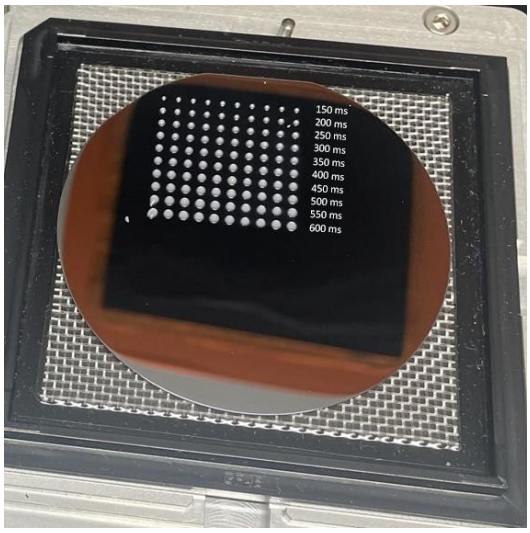

Figure 17: 100 adhesive droplets dispensed on silicon substrate at different pressure application times

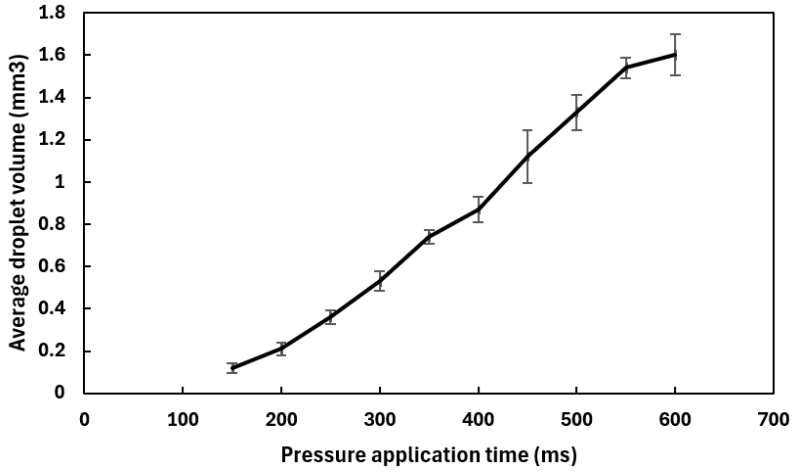

Figure 18: Dispensed droplet average volume Vs pressure application time

The graph shows a linear relationship between the pressure application time and the average volume of the dispensed adhesive droplet. It is also observed that the uniformity decreases as the pressure application time increases. This can be explained as the distance between the dispensing tip and the substrate was held constant at 250 μm. Hence, for the high-pressure application time that produces bigger droplet volumes, the drops were immersed and touched the dispensing tip. Therefore, every drop had some waste that got stuck to the tip which makes the drop volume not as uniform as the small droplets where the drop is completely beneath the dispensing tip as shown in Figure 19.

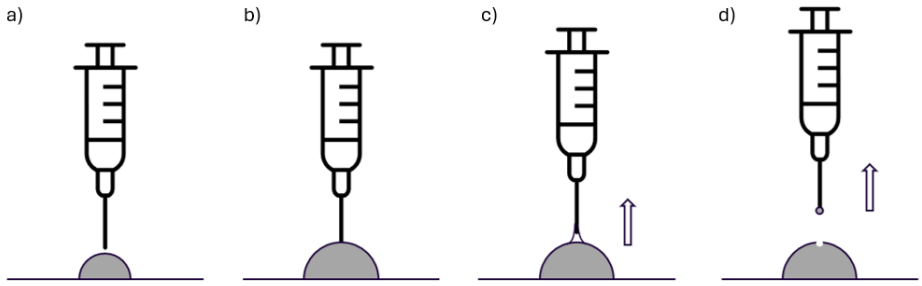

Figure 19: a) Dispensed adhesive height is less than the tip-substrate distance. b) Dispensed adhesive height is more than the tip-substrate distance. c) Some adhesive staying on the surface of the dispensing syringe tip while syringe is moving upwards. d) Dispensed volume decreased due to adhesive pulled by the syringe tip.

Based on these results, it was concluded that the pressure application time that would be used during the assembly process is 150 ms. This application time contributes to dispensed droplets with an average of 0.12 mm3. This was decided so that the volume shrinkage would be minimal. After 150 ms pressure application time was chosen, a separate experiment was done to confirm its results. The experiment followed the same procedure; however, the number of batches was reduced to 5 batches and 5 droplets per batch while the pressure application time was fixed at 150 ms. After dispensing 5 batches with 5 droplets per batch as shown in Figure 20, a total of 25 droplets were dispensed on the silicon substrate with an average volume of 0.12 mm3, which agrees with the results achieved previously.

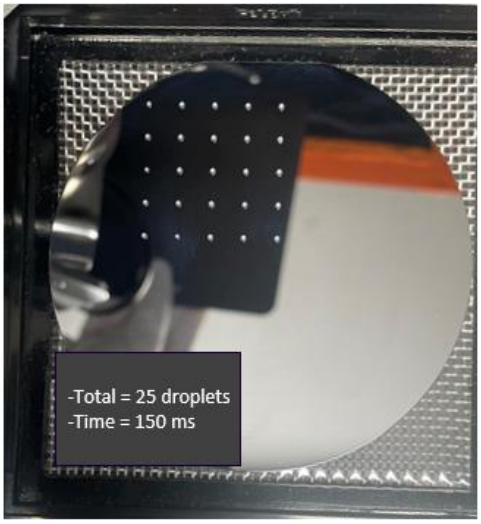

Figure 20: 25 adhesive droplets dispensed on silicon substrate at a pressure application time = 150 ms

Therefore, using DB-OB786 which has a volume shrinkage of 1.6% as the adhesive for the assembly, leads to approximately a volume shrinkage of $0.12 \times \frac{1.6}{100} = 0.002$ mm^3. Assuming that the adhesive has a uniform shrinkage, it means that curing the adhesive will bring the assembled parts closely by approximately 2 µm. This was taken into account that a 2 µm gap is added to the optimized gap between the chips during the active alignment.

2.3.3 Experiment 2: Curing Optimization

The assembly machine includes a 365nm UV LED for adhesive curing. The three parameters that determine the curing profile of the adhesives are the exposure time, the percentage of the power of the UV LED, and the working distance, which is the distance between the UV LED and the dispensed adhesives. As defined, curing is the process of converting the adhesive from its soft or liquid state to a solid one. In addition, curing shrinkage which indicates the negative change of the volume of the cured adhesive, based on the dispensing parameters experiment, was estimated to be around 2 µm^3 using 150 ms pressure application time for dispensing the adhesive droplets. The objective of this experiment was to determine the optimal curing time for UV-curable adhesive DB-OB786 to ensure it is neither over nor under-exposed, ensuring a strong bond during the assembly process.

Experimental Variables

Independent Variables:

- Exposure time
- Working distance: distance between the UV LED and the dispensed adhesive
- UV LED power

Dependent Variables:

- Adhesive curing status: not cured, partially cured, or fully cured

Controlled Variables:

- adherend material: AlN submounts
- Dispensing syringe
- Adhesive type: DB-OB786
- Syringe tip diameter: 0.41 mm
- Number of dispensed drops at the submount side surface: 2 drops
- Distance between the 2 drops: 2 mm
- Environmental conditions: Temperature and humidity
- Pressure application time to dispense adhesive droplets: 150 ms
- Distance between tip and submount to dispense the adhesive: 250 µm

Experimental procedure

Two AlN submounts with the same design for the assembly were used, however, no PIC nor RSOA on top of them was included. One submount was bonded on the aluminum part using silver epoxy, and the second submount was left free to be aligned through the PUT. To have a reference, the isolation black strip was used as an alignment element where both strips from the submounts were to be aligned together as shown in Figure 21.

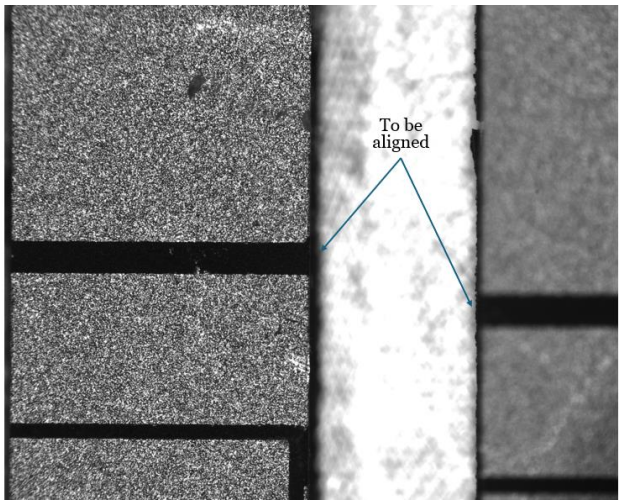

Figure 21: Two AlN submounts to be aligned through their black isolation strips

Based on the adhesive DB-OB786 datasheet, it requires 3-10s to be fully cured at 1 W/cm². From graph X, a working distance between the UV led and the sample was chosen to be 30mm. This distance was chosen to have a uniform irradiation area up to 4 mm² which covers both dispensed droplets as the distance between the two drops was fixed to be 2mm. The following calculations were made to know the theoretical range for curing the adhesive.

For the minimum energy dose required 1 W/cm² × 3s = 3 J/cm²:

Using 10% of the UV LED intensity at a working distance of 30mm, I = 2.4 × 0.1 = 0.24 W/cm²

$$3\ W/cm^2 \cdot s = 0.24\ W/cm^2 \times Time\ (s)$$

$$Time\ (s) = 3/0.24\ (s) = 12.5\ seconds$$

For the maximum energy dose required 1 W/cm² × 10 s = 10 J/cm²:

Using 10% of the UV LED intensity at a working distance of 30mm, I = 2.4 × 0.1 = 0.24 W/cm²

$$10\ W/cm^2 \cdot s = 0.24\ W/cm^2 \times Time\ (s)$$

$$Time\ (s) = 10/0.24\ (s) = 42\ seconds$$

Hence, it was concluded that the curing time ranges between 12.5 - 42 s at a UV LED working distance of 30mm.

First Trial:

The submounts were aligned and positions were saved before the free submount was removed to give space for the dispenser. Then two drops were dispensed as shown in Figure 22 at 150 ms pressure application time on the side surface of the submount.

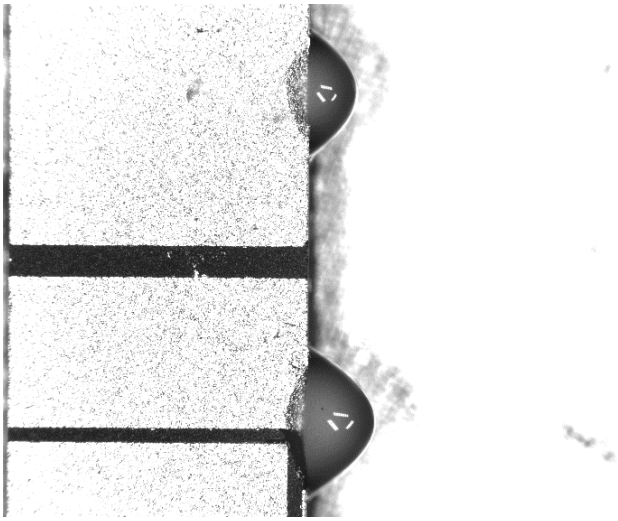

Figure 22: Two adhesive droplets dispensed at the side surface of AlN submount

The free submount was brought back to the alignment position as shown in Figure 23 before starting the curing process.

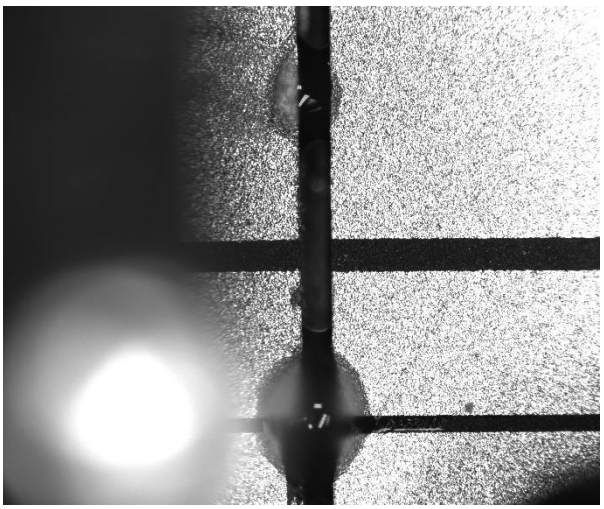

Figure 23: Two AlN submounts aligned by the PUT before adhesive curing

Curing was chosen to be done in 3 steps with 5 s each with a total of 15 s at a working distance of 30 mm with 10% UV LED power intensity. After that, the PUT was moved to observe if the submount was bonded or not. It was observed that the adhesive was fully cured as the PUT couldn't move the submount. Finally, PUT vacuum was turned off and PUT was completely removed as shown in Figure 24.

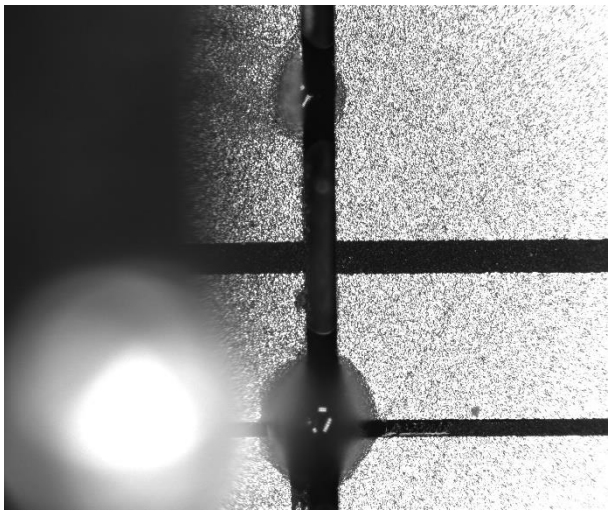

Figure 24: Two AlN submounts final alignment after adhesive full curing

It was shown that the adhesive was fully cured with an energy dose of a little bit more than the minimum required dose. It is also worth noting the subtle movement of the free submount towards the opposite submount. This observation also aligns with the conclusion of the dispensing parameters experiment which assumes that the volume shrinkage will contribute to approximately 2 um movement towards the other chip.

However, further trials were needed to have an optimum curing profile for the assembly process. Since there are some uncontrolled parameters during the assembly process, it was required to do light curing steps that would enable recovering the alignment before the adhesive is fully cured. Those uncontrolled parameters include the gap between the submounts, the droplet distribution across this gap, and finally, the misalignment that happens due to the volume shrinkage.

Note: Typical times for various experimental steps are as follows: Assembly process— 1-2 hours and curing steps —5-10 minutes. It is also worth noting that 5 trials with different curing profiles were needed to reach the optimum curing profile for this project.

Optimum curing profile

To determine an optimal curing profile, trials using the previous experimental procedure were replicated with lower energy doses and shorter curing steps. After several trials with different combinations of power, exposure time, and working distance, the optimum curing profile was established as follows:

UV LED working distance: 50mm

Stage 1: 20 steps at 1% UV LED power intensity for 5 seconds each (allows fixing any misalignment).

Stage 2: 20 steps at 1% UV LED power intensity for 10 seconds each (ensures stable alignment).

Stage 3: 5 steps at 5% UV LED power intensity for 5 seconds each (ensures partial curing before removing PUT).

UV LED working distance reduced to 30mm for higher energy doses for final curing.

Stage 4: 3 steps at 5% UV LED power intensity for 5 seconds each (ensures full curing of the adhesive).

Results and Discussion

The initial trial indicated that a curing time of 15 seconds at a 30mm distance with 10% UV LED power intensity was sufficient for a strong bond, as the adhesive was fully cured. However, to account for uncontrolled parameters during the assembly process, further trials with a detailed curing profile were necessary. The established optimum curing profile ensures controlled alignment and strong bonding, with the flexibility to adjust for any misalignments during the process. The use of controlled steps and varying UV intensities provided a reliable curing method, ensuring the adhesive was neither over- nor under-exposed. This detailed experimental approach ensures the reliability and efficiency of the adhesive curing process, essential for maintaining the integrity and performance of the assembled laser system.

2.3.4 Assembly Process Automation

To ensure that the assembly process is repeatable in a reliable way, the assembly machine was programmed to operate in a semi-autonomous manner. After achieving reliable results from the gluing process experiments, the first step before doing

assemblies was to program the assembly machine. The whole process was planned in a flowchart as shown in Figure 25 before programming the machine.

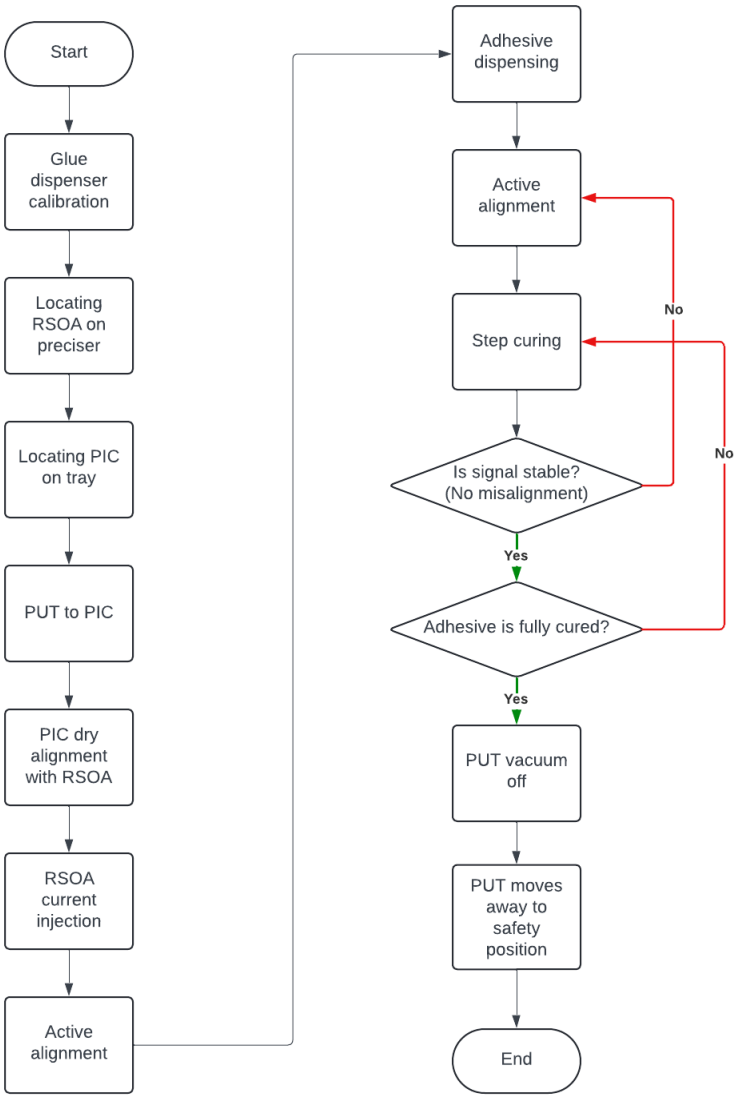

Figure 25: Full assembly sequential process - flow chart

The machine is calibrated in a way that makes it capable of locating the 3D coordinates of any point inside the machine through its vision system. Hence, the first step required is to do a calibration for the adhesive dispenser, which locates the 3D coordinates of the tip of the dispenser. The following steps also include a vision detection which is done through the top camera to locate the chips to be coupled. In this project, this applies firstly to the RSOA on the preciser which is to be fixed without movement through the whole assembly process, and secondly to the PIC which is to be moved freely using the PUT. After locating both chips, the PUT moves to pick the PIC through its vacuum suction. Then the PUT takes the PIC and gets it closer to the RSOA for initial alignment. Current is to be injected in the RSOA before starting the active alignment to find the optimum position for the PIC so that coupling is efficient, and the photodiode signal is the highest. Then the adhesive will be dispensed in the two spots located between the

side surfaces of the submounts of the RSOA and the PIC. Adhesive dispensing accompanies vibrations and some applied forces which introduce misalignment. Hence, active alignment is to be done again. However, the second active alignment will be very fine as the misalignment is usually a few µms. Then step curing starts while observing the signal intensity. If the signal intensity decreases significantly, another fine active alignment is to be done to get back to the highest intensity. This loop is to be going until the signal is stable and the adhesive is fully cured, which means that the bond between the two submounts is strong enough to turn off the vacuum of the PUT. Finally, the PUT is to be removed to go back to its safety position and the assembled parts are to be taken to the lab for characterization.

2.4 Characterization and Packaging

2.4.1 Hybrid Laser Characterization

The characterization of the hybrid assembly was designed to be compared to the lab results achieved by Zia and Ojanen [15] for the same device before the UV adhesive assembly. This was done to be able to evaluate the impact of the UV adhesive assembly on the laser's performance. Key metrics were chosen to be light-current (LI) characteristics, wavelength emission, lasing threshold, and output power. The aim of the characterization phase is to determine whether the post-assembly hybrid laser maintains, exceeds, or potentially falls short of the performance benchmarks set by the pre-assembly laser.

Firstly, LI measurement represents the core characterization metric of the hybrid laser as it shows the current threshold, and the maximum output power, both adversely affected by any misalignment. To do LI measurements, probes are used to inject current into the RSOA. Keithley's source measurement unit (SMU) [21] is used to inject the current. In addition, a photodiode is put very close to the output of the laser to detect the output power. Then current is swept for a specific range while the photodiode measures the output power using Thorlabs' optical power meter [22] at the same time. The threshold is then registered when there is a jump in the power level at a specific injected current. Hence, the first point that has the highest slope is considered to be the threshold current. The maximum output power is registered as the highest point of the curve which corresponds to the highest signal received by the photodiode at a specific injection current. A typical setup of LI measurements is presented in Figure 26.

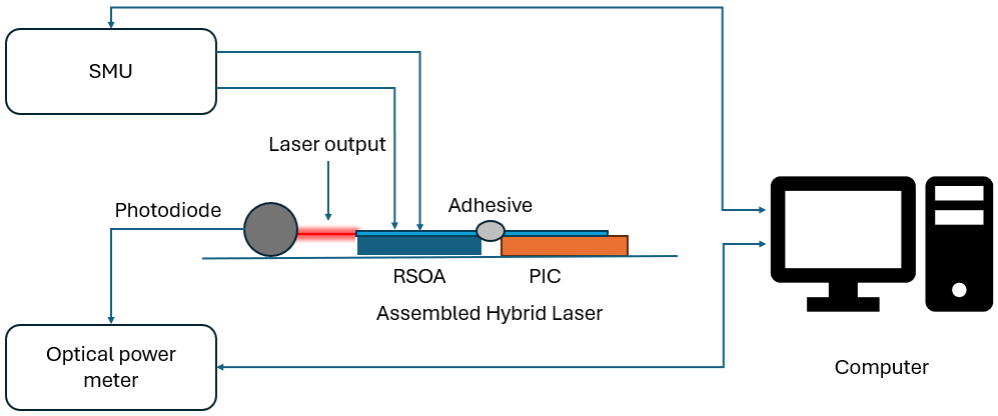

Figure 26: Schematic of LI measurement setup

Secondly, to measure the wavelength emission, an Optical spectrum analyzer (OSA) is used. OSA measures the spectrum of the output light from the laser. Hence, in addition to injecting current into the RSOA, electric power is injected into the PIC to tune the wavelength. The output light is transferred from the laser to the OSA through a single-mode fiber (SMF) to measure the spectrum at each input power to characterize the wavelength emission of the assembled laser. The wavelength emission measurement setup is shown in Figure 27.

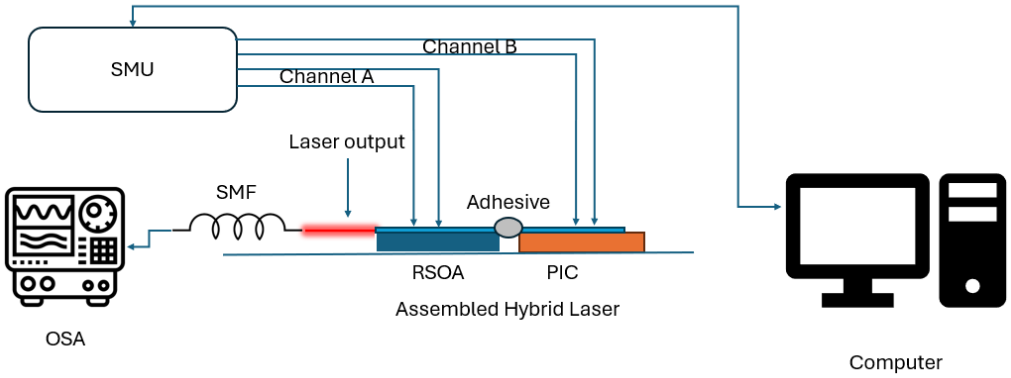

Figure 27: Schematic of wavelength tuning range measurement setup

2.4.2 Butterfly Packaging Process

Repeatable and reliable packaging is crucial to meet the cost and performance aims of the tunable hybrid lasers. Manual assemblies result in low yield and limit the applicability of mass production. Hence, the main objective for packaging is to complete the last step for production automation to transition the assembled laser from a laboratory setting to real-world usage, ensuring it can withstand operational stresses and maintain its performance over time. Moreover, it addresses thermal management challenges, as the different materials used in the laser may have varying thermal expansion coefficients. Hence, it ensures that the thermal stability of the system is maintained using thermoelectric coolers, preventing misalignment and degradation of the laser's performance over time. All the dimensions (in mm) of the chosen standard butterfly package are shown in Figure 28.

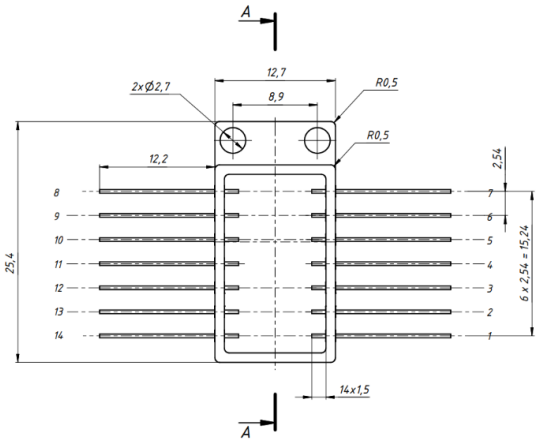

Figure 28: Schematic of the chosen butterfly package

As mentioned in section 2.2.2, the assembly was designed to fit inside the package and also to align the output of the laser with the center of the circular aperture of the package as shown in Figure 29.

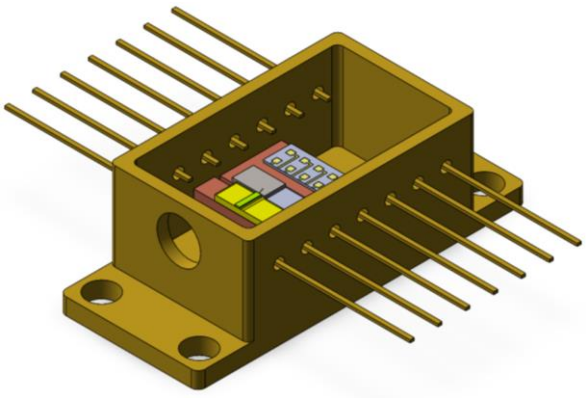

Figure 29: Schematic of the assembly design inside the butterfly package

There are two main challenges in packaging the assembled lasers using UV adhesives. Firstly, the aluminum platform, as the base of the assembled laser, needs to be bonded to the thermoelectric cooler of the package with a high thermal conductivity material at room temperature. This requires the use of a high thermal conductivity underfill that cures effectively at room temperature. Secondly, a converging lens needs to be precisely positioned at the outlet of the package to collimate the laser beam. To achieve this, a platform must be designed to securely hold the lens at the optimal working distance, ensuring a collimated laser beam output.

3. Results

3.1 Assembly Design Outcomes

3.1.1 RSOA/Passive WG assembly

Before proceeding with assembly trials of the 2000 µm wavelength GaSb RSOA and the PIC, it was essential to do assemblies with dummy PICs to verify that the process was designed properly. This is because PICs in this case are very valuable components as they are not manufactured in volume while dummy chips could be made from GaSb with ease at TAU (By Mr. Samu-Pekka Ojanen). Thus, GaSb RSOAs with emission of 1700 µm were used as passive WGs at the main RSOA emitted wavelength of 2000 µm. The active GaSb RSOA that will be injected with the current has a length of 2000 µm and a chip width of 450 µm. This will provide gain and cavity feedback for the two assembled lasers; the laser that uses a passive WG for assembly trials and the tunable laser that uses a Si_3N_4PIC. The RSOA has a single-mode ridge waveguide (RWG) with a 5 µm width and a "J-shaped" structure. In addition, as shown in Figure 30, the WG is bent with a 7° output angle at the front facet and an anti-reflection (AR) coating to maximize the output [14].

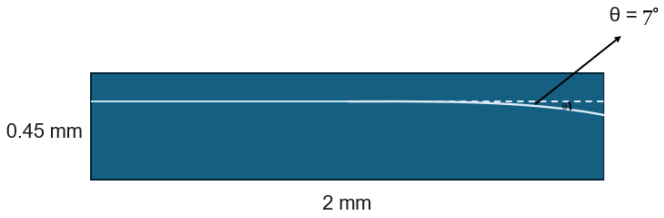

Figure 30: Schematic of the GaSb RSOA chip

While the active GaSb RSOA is referred to as RSOA, the other GaSb RSOA that will be used as a passive chip, is referred to as a passive WG through the process. The assembly started by putting the RSOA with the current injection platform on the preciser as shown in Figure 31.

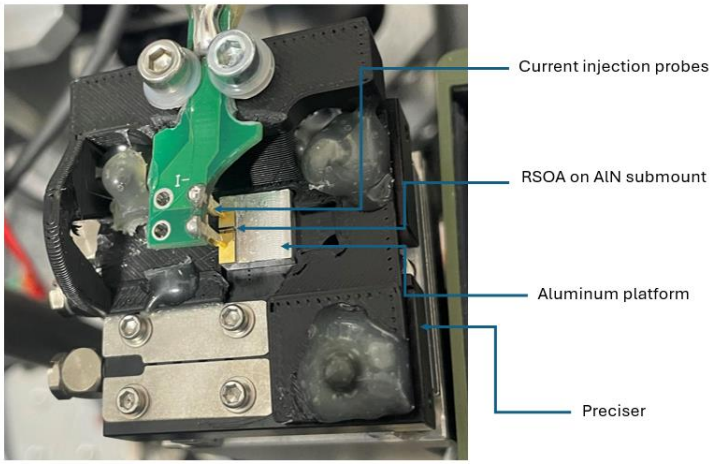

Figure 31: Assembly platform on top of the preciser with probes injecting current into the RSOA

The current was injected, and the photodiode signal was observed to check that the probes were injecting current to the RSOA properly. After that, the top camera moved to locate the coordinates of the RSOA WG as shown in figure 32.

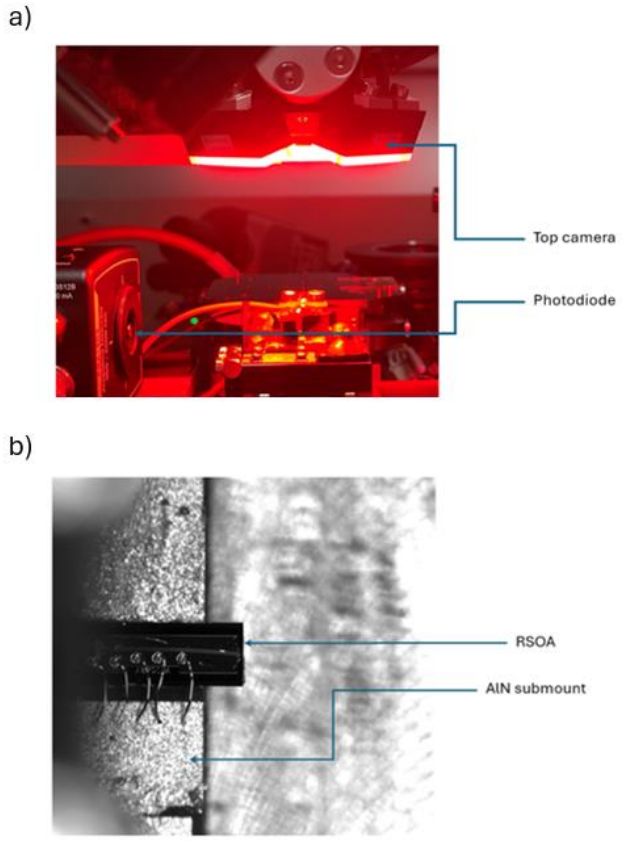

Figure 32: a) top camera locating the RSOA chip. b) Image taken by the top camera.

Afterward, the top camera moved to locate the passive WG so that it could be picked up by the PUT as shown in Figure 33.

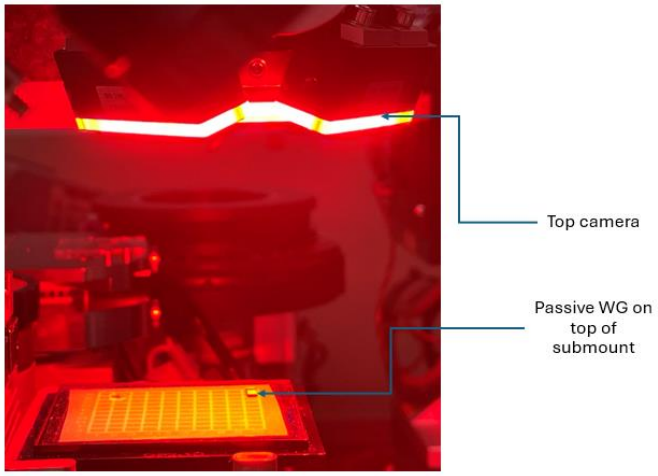

Figure 33: Top camera locating the passive WG chip

Then the vacuum suction of the PUT is turned on before it grabs the submount with the passive WG on top as shown in Figure 34.

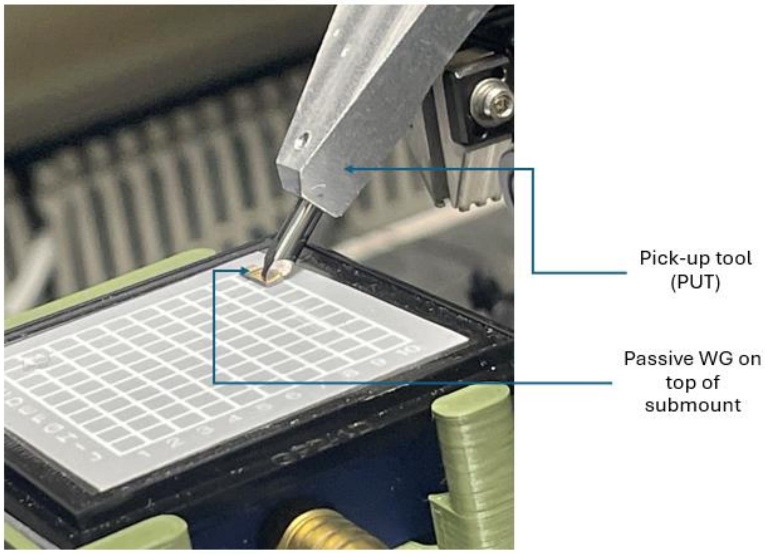

Figure 34: PUT holding the AlN submount with the passive WG on top

Following that, the PUT moved toward the RSOA's submount to prepare the passive WG and the RSOA for a dry alignment. Both chips got closer before dry alignment as shown in Figure 35.

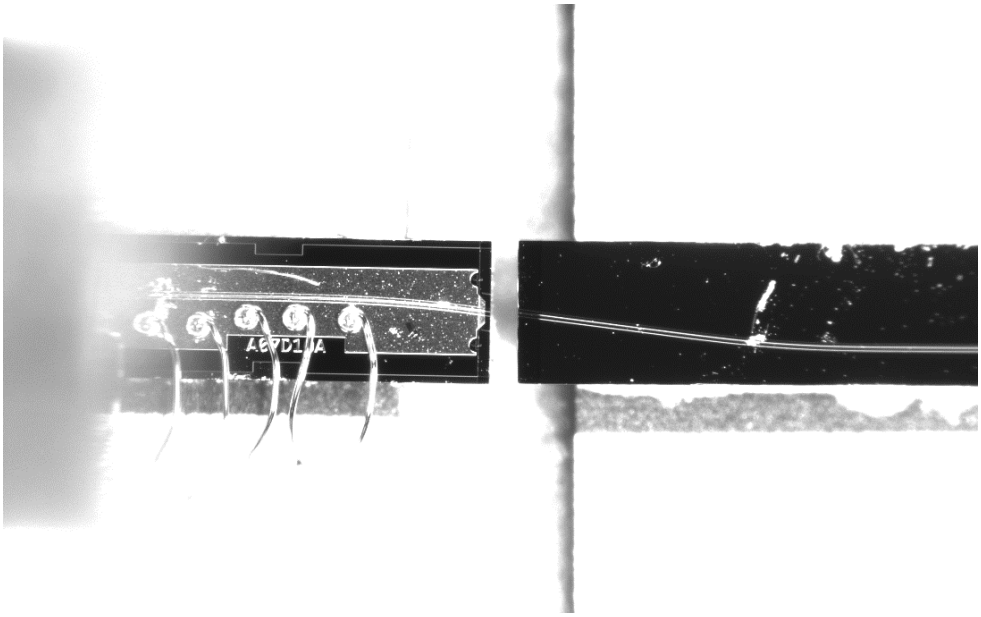

Figure 35: Initial alignment between the RSOA and the passive WG

Then the current was injected into the RSOAs through the probes and both WGs were put as close as possible as shown in Figure 36.

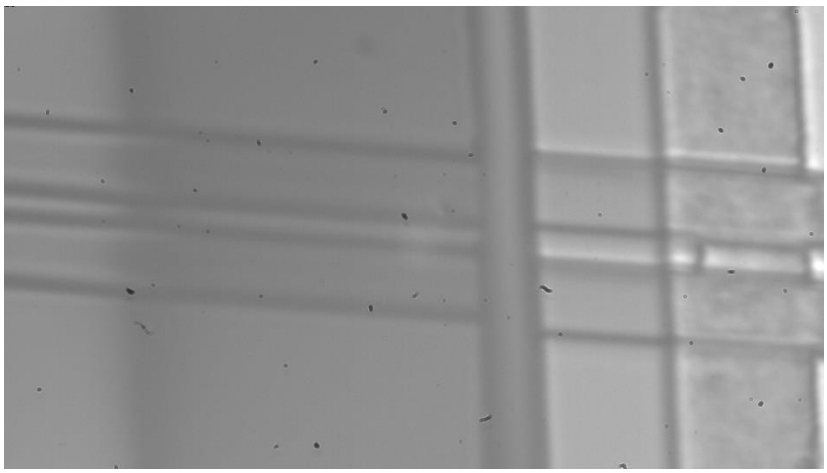

Figure 36: Initial alignment of the WGs before active scanning

In order to find the optimum alignment position, active scans were done. Those scans entailed coarse and fine sweeping of the passive WG in Y and Z directions while observing the photodiode signal until the maximum is found. Firstly, the coarse alignments included three scans. As shown in Figure 37.a, a quick scan of 50 µm in the z-axis and 10 µm in the y-axis. The PUT moved accordingly to put the passive WG on the coordinates that achieved the maximum signal. Then the process was repeated with two different scan profiles. As shown in Figure 37.b, the second scan spanned a smaller area of 20 µm in the z-axis and 10 µm in the y-axis. Then the final scan at this stage spanned an area of 5 µm² as shown in Figure 37.c.

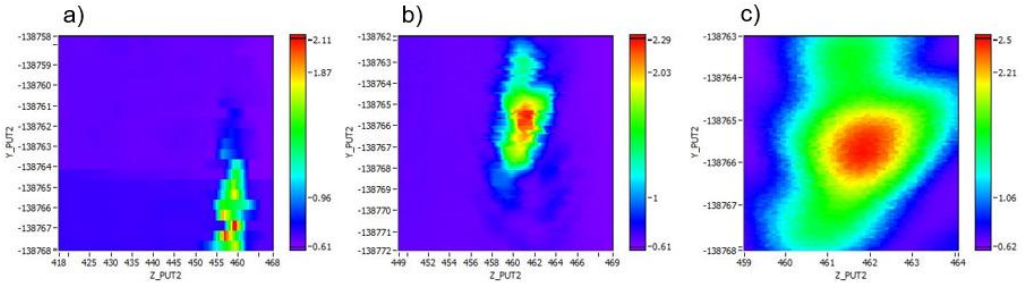

Figure 37: Active alignment scannings. a) 50 µm in z-axis and 10 µm in y-axis. b) 20 µm in z-axis and 10 µm in y-axis. c) 5 µm in z-axis and 5 µm in y-axis.

It was observed that as the scan got finer, the local maximum was higher and clearer. The PUT held the passive WG at the position where the local maximum was achieved. Afterward, two droplets of the selected adhesive (DB-OB786) were dispensed at a pressure application time of 150 ms. It was observed that using a straight tip to dispense droplets at the gap between the adherends is more practical than using bent tips. Using bent tips required to move the free chip away, which contributed to losing the alignment. Hence, it was decided to use straight tips and dispense the adhesive from the top while both chips were held in the position of alignment. Adhesive droplets were dispensed 2 mm away from each other at the gap between the submounts as shown in Figure 38.

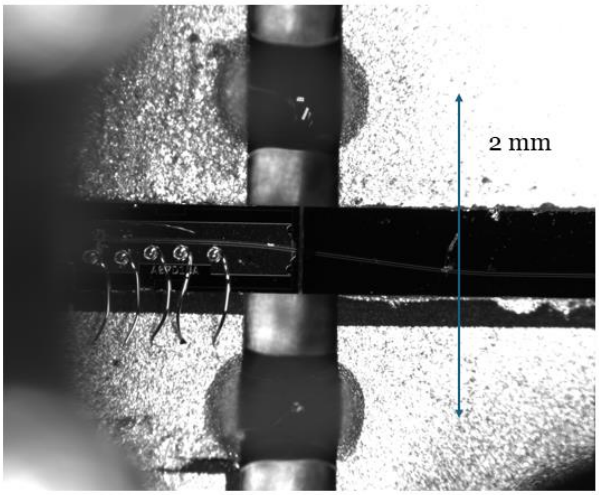

Figure 38: 2 mm away dispensed adhesive droplets at the gap between the AlN submounts

Dispensing the adhesive entailed a little misalignment due to the high viscosity of the adhesive. Hence, a final fine active scanning was required. The fine scan spanned area of 3 µm² and 2 µm² in z and y axes as shown in figure 39.a and 39.b respectively.

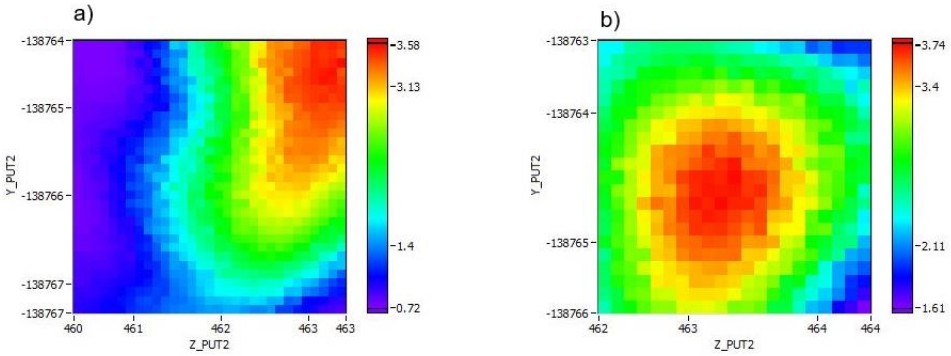

Figure 39: Active alignment scannings. a) 3 µm in z-axis and 3 µm in y-axis. b) 2 µm in z-axis and 2 µm in y-axis.

The local maximum was higher and clearer with the finest scan of 2 µm2 as shown in Figure 39.b, however, the local maximum was significantly higher than the local maximum achieved before dispensing the adhesive droplets. This can be explained that due to the high viscosity of the adhesive, the two submounts got closer, minimizing the gap between the two WGs. The gap between the chips was increased by 0.5 µm to mitigate the shrinkage effect during curing.

Afterward, the UV LED was brought on top of the dispensed adhesive droplets to cure them. The distance between the LED and the droplets was fixed at 50 µm during the initial curing steps and towards the end this distance was decreased to 30 µm to make the final curing steps. During the curing process, the photodiode signal was observed to know if active scans were required to fix any misalignment. The signal during the whole assembly process is shown in Figure 40.

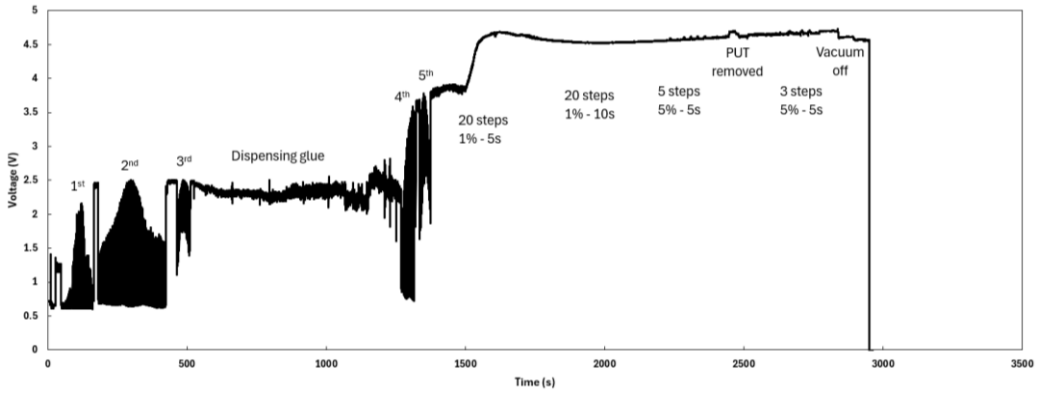

Figure 40: Photodiode detected signal over time through the whole assembly process

This graph shows how the signal of the photodiode changed during various stages of the assembly process. The minimum value of 0.6 V represents the emitted light from the RSOA only. The first three active scans titled according to their order, are shown, and they have Gaussian shapes with the maximum peaks representing the highest signal achieved at each scan. The maximum value achieved before dispensing the adhesive was 2.5 V. The signal during the dispensing of the adhesive carried some noise, which is normal to observe due to the vibrations of different parts of the assembly machine to be able to dispense the adhesive. After that, the final two fine scans titled 4th and 5th according to their order, showed a maximum of 3.74 V. After the final alignment, curing started with 20 steps of 1% of the power of the UV LED for 5 seconds each. During those small curing steps, a significant increase in the signal which reached up to 4.6 V was observed. This increase can be attributed to the shrinkage of the adhesive which approximately brought the two WGs closer by 2 μm, which made the chips even closer than the optimum alignment before curing. Afterward, the rest of the steps of the curing profile were done as concluded from the curing experiments. A small decrease in the signal happened after removing the PUT, which can be explained by the relaxation of the adhesive after the PUT was removed. Hence, the signal maintained a stable signal of 4.58 V after passing all the assembly process steps. Finally, the current injection was stopped, and the signal went back to 0 V before picking up the assembled laser for lab measurements and characterization.

Note: The full assembly process takes 2-3 hours. It is also worth noting that 7 assembly trials with passive WG were needed to automate the process before doing 5 successful assembly trials.

Using probe needles, continuous wave (CW) current was injected into the GaSb RSOA. The assembled laser was put so that the output signal was measured by a photodiode as shown in Figure 41.

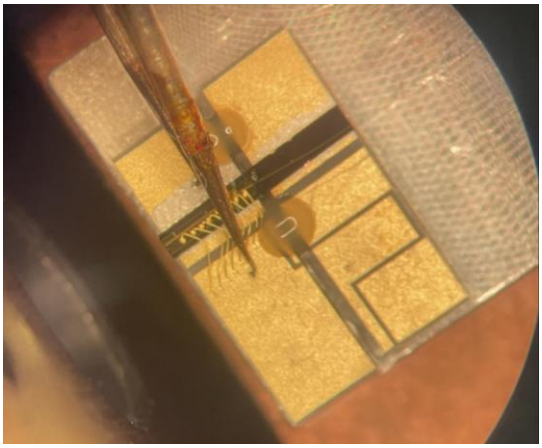

Figure 41: Assembled laser output put close to the photodiode for LI curve measurement

The current was swept from 0 to 350 mA, and the light-current (LI) curve was measured as presented in Figure 42.

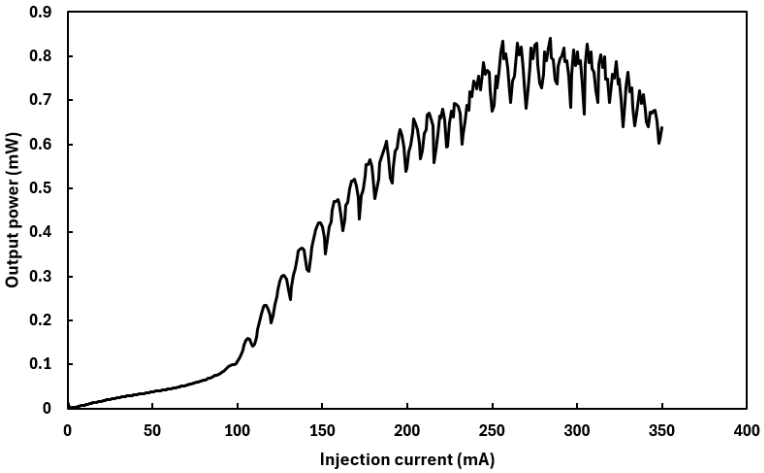

Figure 42: LI curve measured immediately after the assembly

The assembled laser had a threshold current of approximately 100 mA. In addition, a maximum CW output power of 0.84 mW was achieved at an injection current of 284 mA. It is observed that the power oscillates while the injection current is increasing beyond the threshold value. This can be referred to as the direct relationship between the temperature of the active region of the RSOA and the injection current. Hence, increasing the current led to an increase in the temperature, which contributed to variation in the refractive index through the thermo-optic effect. Consequently, the phase of the RSOA kept changing while the phase of the passive WG did not change, which led to the power oscillations shown in Figure 42.

The same measurements were repeated after 1, 4, and 6 days to evaluate the long-term stability of the assembled laser. Clear degradation in maximum power values were observed as shown in Figure 43.

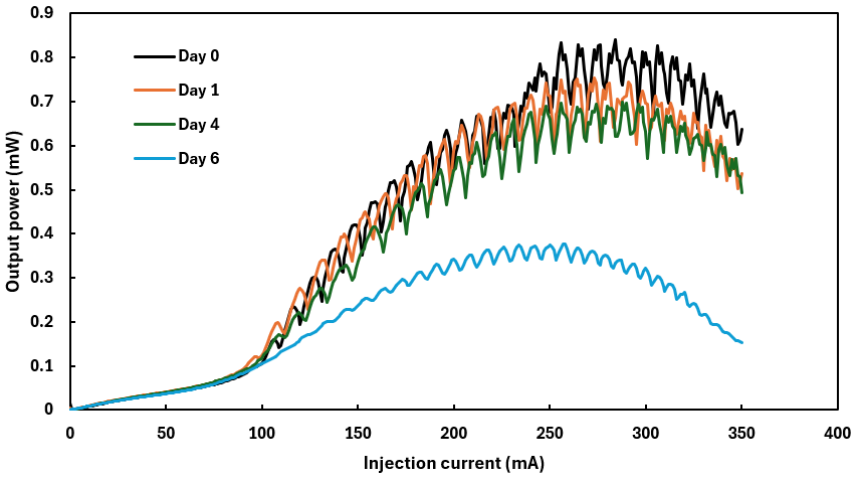

Figure 43: LI curve measured at different times. Black - immediately after assembly, Orange - after 1 day, Green - after 4 days, Blue - after 6 days.

As observed in Figure 43, the maximum output power dropped from 0.84 mW on day 0 to 0.37 mW on day 6. This could be either due to the relaxation effect of the cured adhesive which increases the gap between the chips, or due to the fact that the passive WG's submount does not have enough mechanical support. The relaxation effect happens when the polymeric chains of the adhesive rotate around each other to have the same direction and bending. At this stage, the relaxation effect could not be mitigated as the adhesive was fully cured. Hence, two droplets of the same adhesive were dispensed at the backside of the submount to increase its mechanical stability as shown in Figure 44.

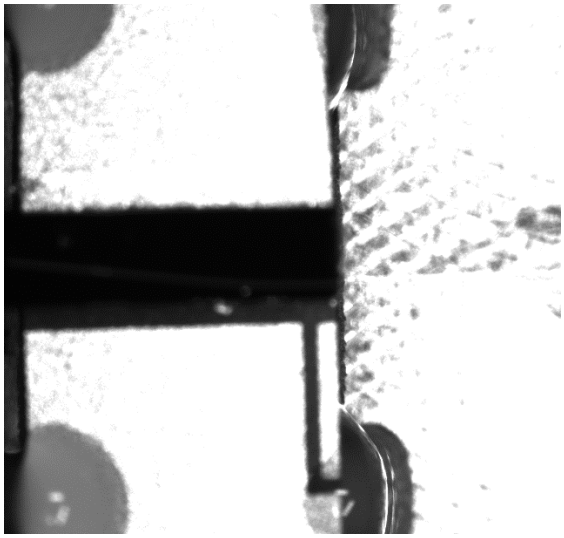

Figure 44: Two adhesive droplets dispensed at the backside of the passive WG submount

To evaluate that the new droplets would decrease the degradation of the assembled laser over time, LI curve measurements were done immediately after the adhesive was dispensed and one week later. It was observed that the back support that the adhesive provided not only eliminated the degradation over time but also showed some recovery as the output power levels increased as shown in Figure 45. Since it was shown that the

assembly is mechanically supported, and no degradation happened over time, it was essential to evaluate if wire bonding would be handled. Hence, wire bonding was done at room temperature, and it is shown in Figure 45, that no power degradation happened to the device.

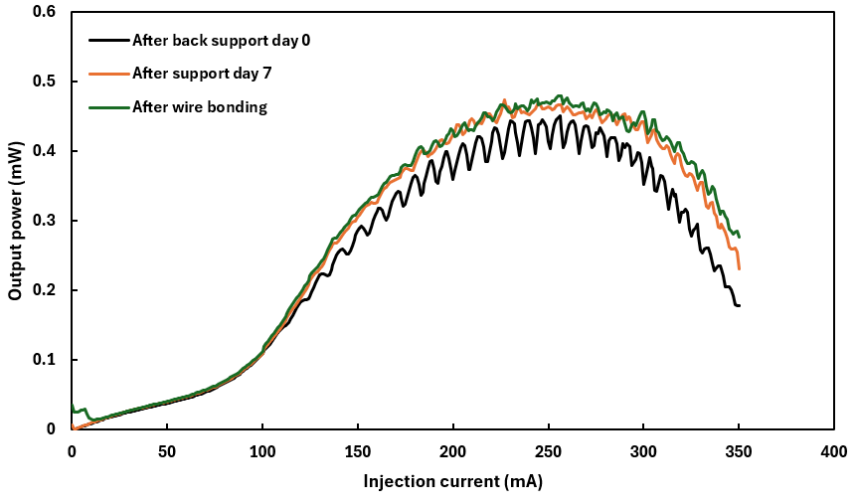

Figure 45: LI curve measurements after provided backside mechanical support. Black - immediately after curing the backside dispensed droplets, Orange - one week later, Green - immediately after wire bonding.

The last challenge to be tackled was the heat dissipation of the passive WG's submount. It was aimed to use silver particle-filled epoxy to fill the gap between the submount and the aluminum platform, however, silver epoxy requires high temperatures of 100-150 °C to get solidified. Hence, the device temperature was raised to 100 °C for 1 hour, which is the minimum condition to solidify silver epoxy at high temperatures. Afterward, LI measurements were done to evaluate the temperature effect on the device's performance. As shown in Figure 46, the device could not handle being exposed to high temperatures as significant power degradation was observed.

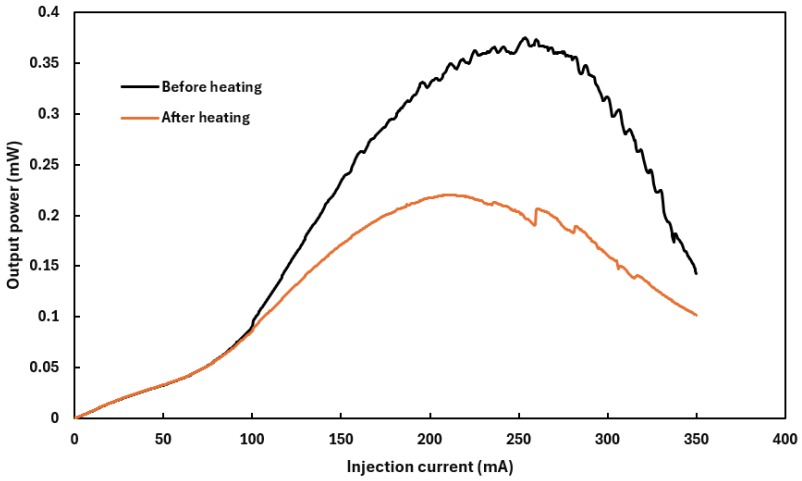

Figure 46: LI curve measurements to assess the laser performance after being heated up. Black - before heating, Orange - after being heated for 1 hour at 100 °C

Hence, it was concluded that underfills that cure at room temperature are to be used to fill the gap under the submount.

To sum up, successful assembly trials of GaSb RSOA and passive WG were shown. LI measurements were used to evaluate the long-term stability of the assembled laser. Due to power degradation over time, additional adhesive droplets were added to offer mechanical stability which contributed to a more stable performance. However, increasing the gap between WGs to mitigate the shrinkage effect did not show its effectiveness. This is due to the relaxation effect which would increase the gap after it was decreased by the shrinkage effect. In addition, a high-temperature test was done to assess the applicability of curing silver epoxy to fill the gap below the AlN submount. Finally, it was concluded that the assembly process is reliable and repeatable.

3.1.2 RSOA/PIC assembly

After repeatable successful assembly trials with the passive WG, assembly trials with Si_3N_4 PICs started. The same process was followed as planned in section 2.3.4 and implemented in section 3.1.1. The RSOA and the PIC were bonded on AlN submounts using silver epoxy. Then to finalize the preparation of both chips before assembly, the RSOA's submount was bonded on the high step of the aluminum platform as discussed in the revised design in section 2.2.2.

After preparing both chips, the top camera was used to locate the corresponding WGs and PUT was used to hold the PIC's submount and bring it closer to the RSOA WG as shown in Figure 47.

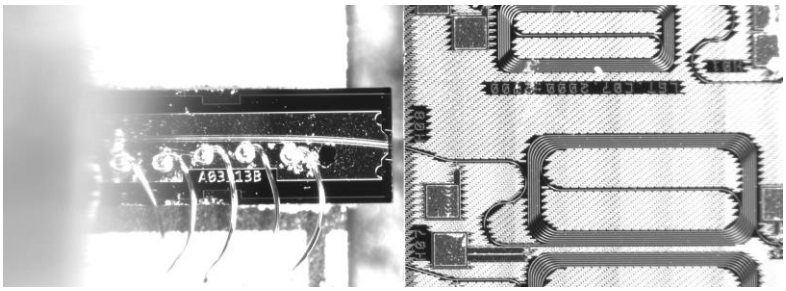

Figure 47: Initial alignment between the RSOA and the PIC chips

Using a microscope lens, the WGs were brought as close as possible for an initial alignment as shown in Figure 48.

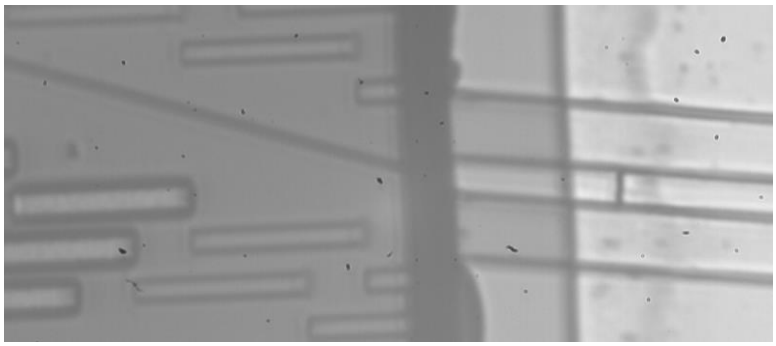

Figure 48: Initial alignment of the WGs before active scanning

Then current was injected into the RSOA, and several scans were done in order to find the highest signal received by the photodiode. The first scan was a quick scan of 15 µm on the z-axis and 10 µm on the y-axis as shown in Figure 49.a, which yielded a maximum signal of 6.53 V. The PUT positioned the PIC WG at the optimum position before starting a finer scan of 5 µm in both directions as shown in Figure 49.b. The signal achieved was 6.46 V, which is lower than what was achieved through the coarse scan. Hence, a finer scan of 2 µm in both directions was made with a smaller step of 0.001 µm as shown in Figure 49.c.

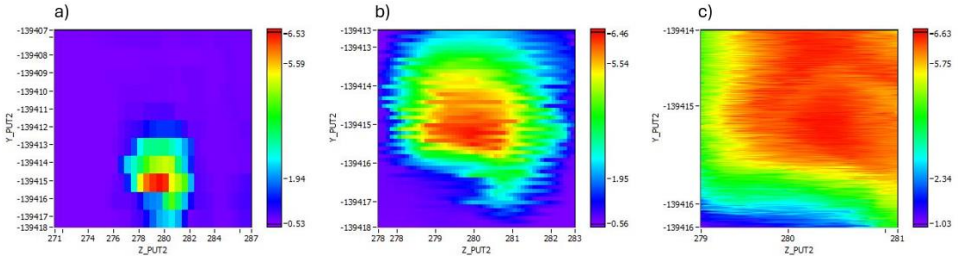

Figure 49: Active alignment scannings. a) 15 µm in z-axis and 10 µm in y-axis. b) 5 µm in z-axis and 5 µm in y-axis. c) 2 µm in z-axis and 2 µm in y-axis.

As shown in figure 50, the PIC was held at the final alignment position which achieved the highest intensity of 6.63 V.

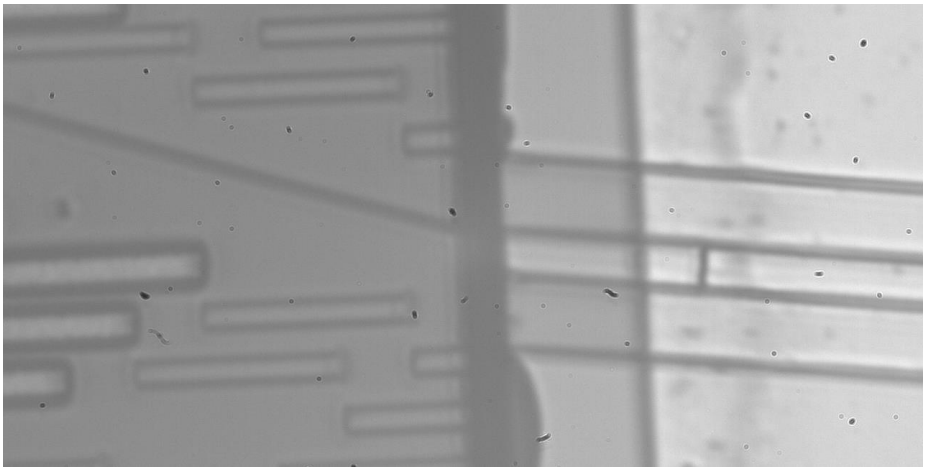

Figure 50: Final alignment before adhesive dispensing

Afterward, two droplets of the selected adhesive (DB-OB786) were dispensed at a pressure application time of 150 ms. Adhesive droplets were dispensed 1.8 mm away from each other at the gap between the RSOA's submount and the PIC as shown in Figure 51.

It was observed in the passive WG assembly that dispensing the adhesive brings the chips closer which increased the intensity of the signal received by the photodiode. Hence, after dispensing the adhesive, two fine scans that spanned an area of 5 µm2 and 2 µm2 in the z and y axes as shown in Figures 52.a and 52.b respectively were done. The observation was once again confirmed, and the finest scan achieved a significantly high-intensity signal of 10.59 V.

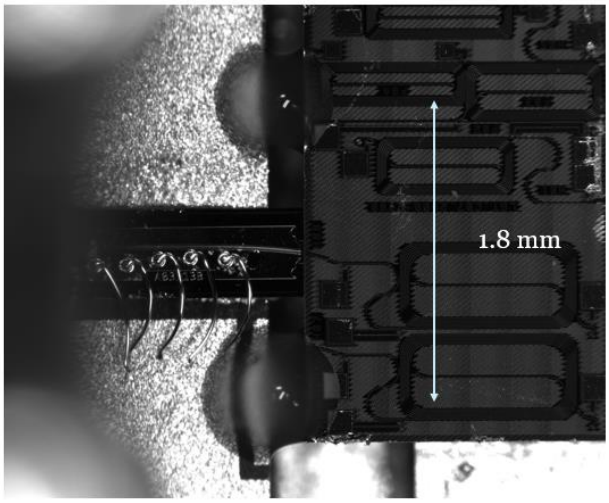

Figure 51: 1.8 mm away dispensed adhesive droplets at the gap between the RSOA's AlN submount and the PIC

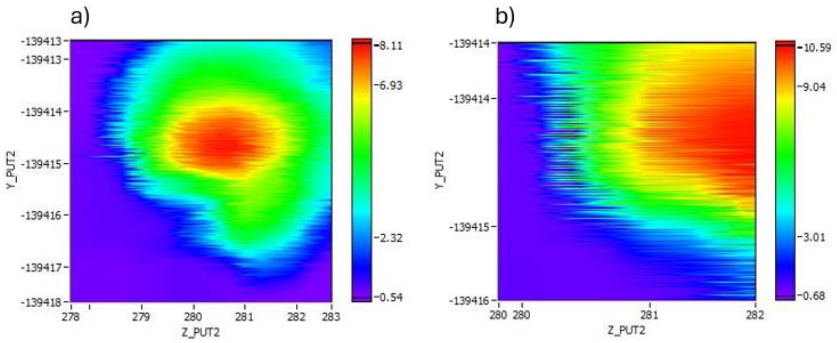

Figure 52: Active alignment scannings. a) 5 µm in z-axis and 5 µm in y-axis. b) 2 µm in z-axis and 2 µm in y-axis.

The signal was very high, and the lock-in amplifier (LIA) used to amplify the signal detected by the photodiode amplified it to the saturation level. Hence, the amplification factor of the LIA was reduced to half to detect larger signals. After that a final scan that spanned an area of 2 μm^2 was done and the local maximum was clear with a value of 5.51 V as shown in figure 53.

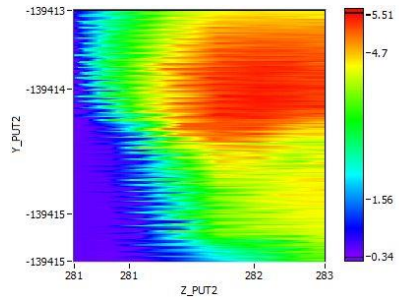

Figure 53: Final active alignment scanning of 2 µm in z-axis and 2 µm in y-axis after reducing the LIA amplification factor by 2

Afterward, the UV LED was brought on top of the dispensed adhesive droplets to cure them. The same curing profile presented in 2.3.3 and used in section 3.1.1 was followed. The signal during the whole assembly process is shown in Figure 54.

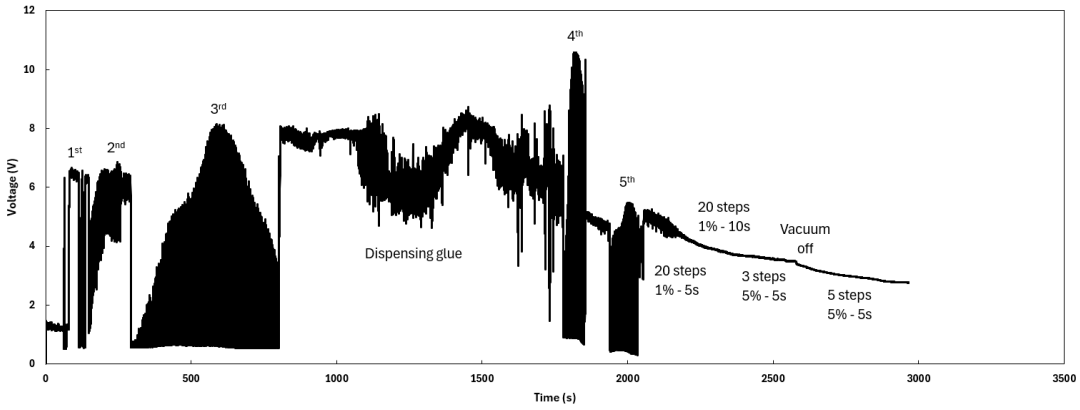

Figure 54: Photodiode detected signal over time through the PIC assembly process

The lowest value of 0.5 V corresponds to the emitted light from the GaSb RSOA only. All the scans are numbered accordingly from the initial scan up to the fifth and last one. After changing the settings of the LIA so that the new maximum is half the maximum achieved, it is observed that the 5th scan had a value that is almost half the value of the maximum reached in the 4th scan. After the final alignment, curing started with 20 steps of 1% of the power of the UV LED for 5 seconds each. During those initial curing steps, a significant decrease in the signal was observed. However, it was decided to proceed based on the observation of the relaxation effect. The rest of the curing steps were completed accordingly as shown in Figure 54. After the final curing steps and removing the PUT, the signal was saturated at around 2.8 V, which is around 50% of the maximum achievable signal. Finally, the current injection was stopped, and the assembled laser was picked up for lab measurements and characterization.

3.2 Tunable Laser Characterization Results

With the same characterization procedure, CW current was injected into the RSOA using probe needles. The tunable laser was put so that the output signal is measured by a photodiode as shown in Figure 55.

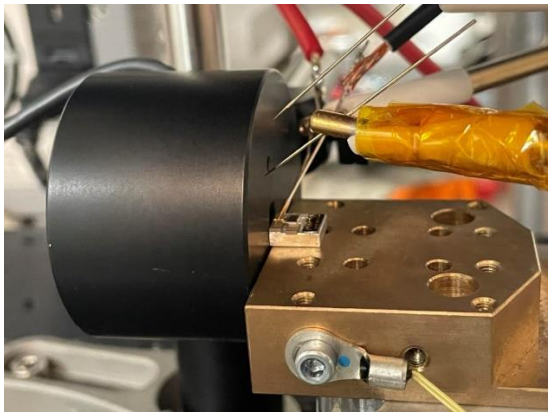

Figure 55: Lab setup to measure the LI curve of the assembled tunable laser

The current was swept from 0 to 300 mA, and the LI curve was measured as presented in figure 56.

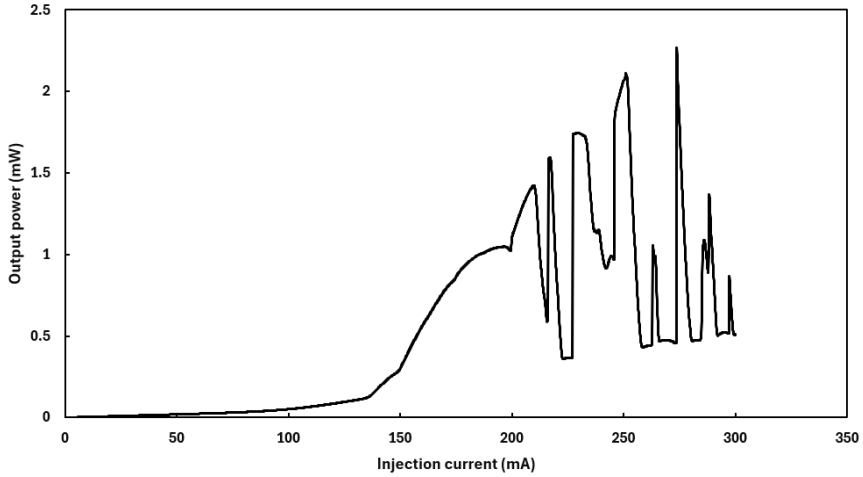

Figure 56: Assembled tunable laser LI curve measured immediately after the assembly

The assembled tunable laser had a threshold current of approximately 137 mA. A maximum CW output power of 2.3 mW was achieved at an injection current of 274 mA. Oscillations were also observed as expected and explained in section 3.1.1. After this measurement, based on results achieved in section 3.1.1, two adhesive droplets were dispensed to support the back side of the PIC's submount as shown in figure 57.

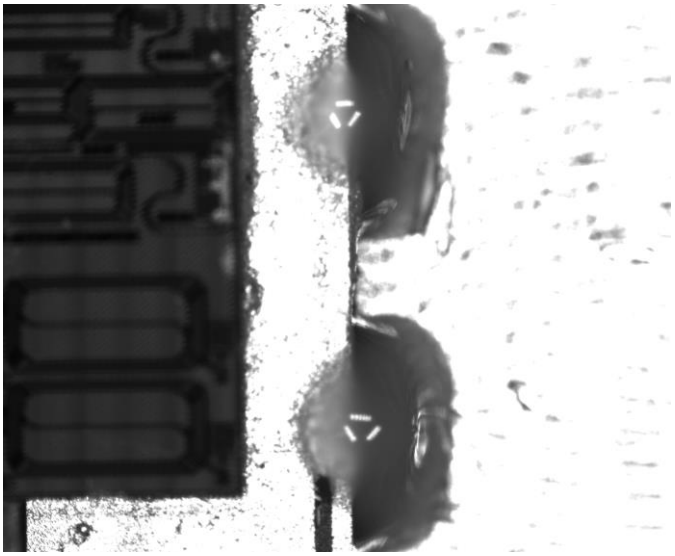

Figure 57: Two adhesive droplets dispensed at the backside of the PIC's submount

The same measurement was repeated immediately after curing those droplets to evaluate if any misalignment happened due to this process. As shown in Figure 58, which compares the IL curve before and after dispensing and curing the back support droplets, a slight shift in the threshold from 137 mA to 145 mA. The maximum power level also dropped from 2.3 mW to 2.1 mW.

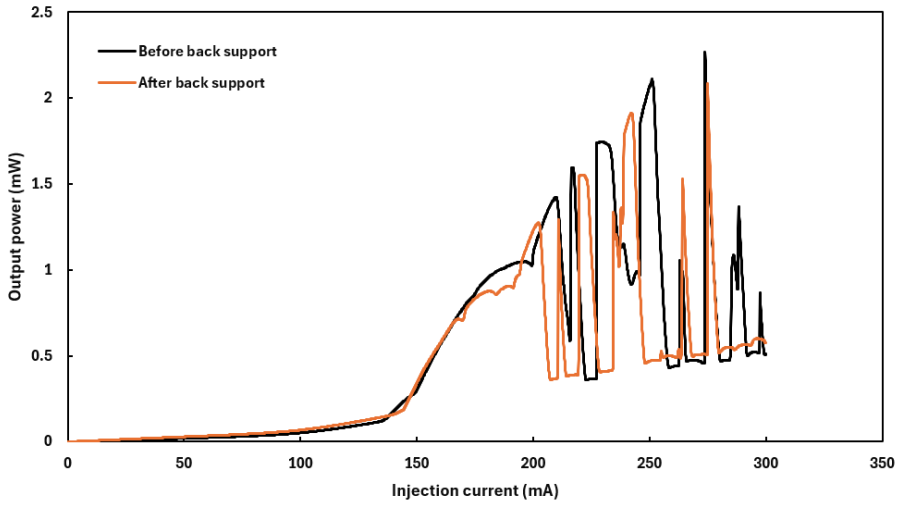

Figure 58: LI curve measurements before and after provided backside mechanical support

To evaluate that the new droplets would decrease the degradation of the assembled laser over time and that the relaxation effect would compensate for the lost signal during curing, LI curve measurements were done immediately after the adhesive was dispensed and one week later. The performance was improved significantly as shown in Figure 59. This can be attributed to the relaxation effect which put the chips back to their optimum alignment position after the gap between them was decreased by the shrinkage effect.

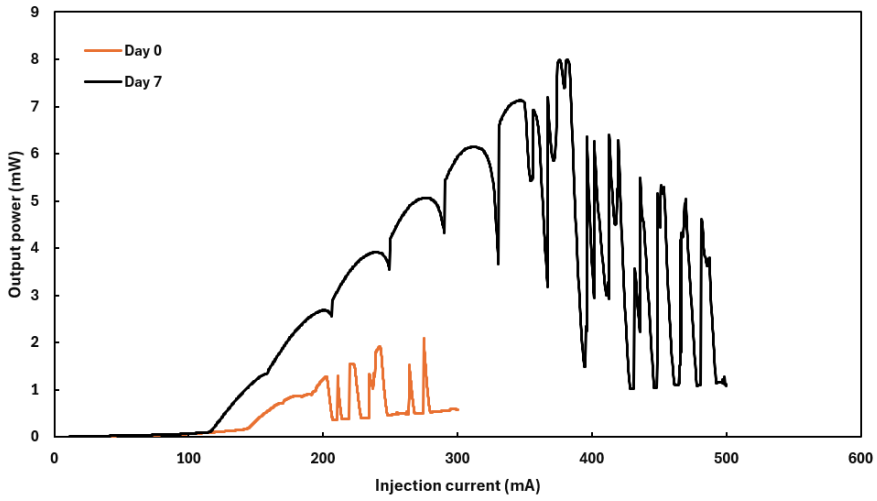

Figure 59: Assembled tunable laser LI curve measured at different times. Orange - immediately after assembly, Black - after 1 week.

The threshold dropped from 145 mA to 117 mA, while the maximum power increased significantly from 2.1 mW to 7.7 mW.

Since it was shown that the relaxation effect improved the performance, and no degradation happened over time, it was essential to evaluate if the assembly was mechanically supported for the wire bonding. Hence, wire bonding was done at room temperature, and it is shown in Figure 60 that neither power degradation, nor current threshold shift happened to the laser.

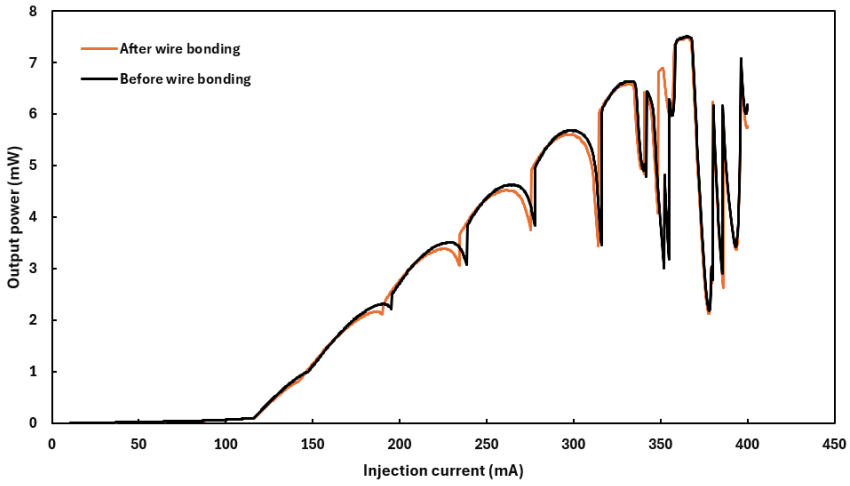

Figure 60: Assembled tunable laser LI curve measured before and after wire bonding

To evaluate the laser's performance after the assembly, the IL curve measurement of the assembled tunable laser shown in Figure 60 was compared to the IL curve measurement of the tunable laser before the UV-adhesive assembly done by Zia and Ojanen [14]. As shown in Figure 61, the assembled laser has a threshold of 117 mA while the laser before assembly has a threshold of 215 mA. In addition, it is noticeable that the UV-adhesive assembled laser reached a higher value of the maximum output power of 7.7 mW while the maximum output power reached before assembly was 5.7 mW. This shows that the performance is satisfactory as the power levels are higher within the same order of magnitude and the current threshold is lower.

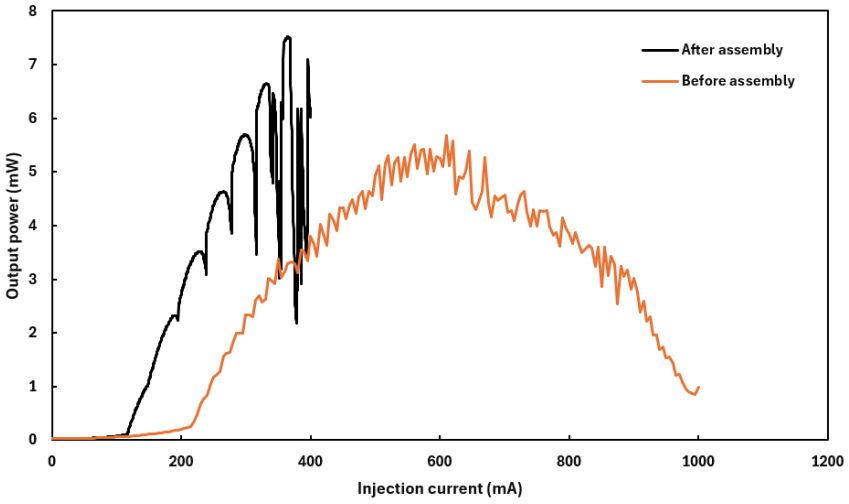

Figure 61: Performance evaluation of the hybrid UV-adhesive assembled tunable laser. Orange - before assembly, Black - after assembly.

As explained in section 3.1.1, increasing the injected current changes the phase of the RSOA which leads to the oscillation observed in Figure 60. In order to match the phase of the RSOA and the PIC, the current was injected into the PIC and LI measurements were done and the maximum output power was selected. The phase matching and non-

matching results are compared in Figure 62, confirming that the power oscillations are due to the RSOA phase changing with increasing the injected current.

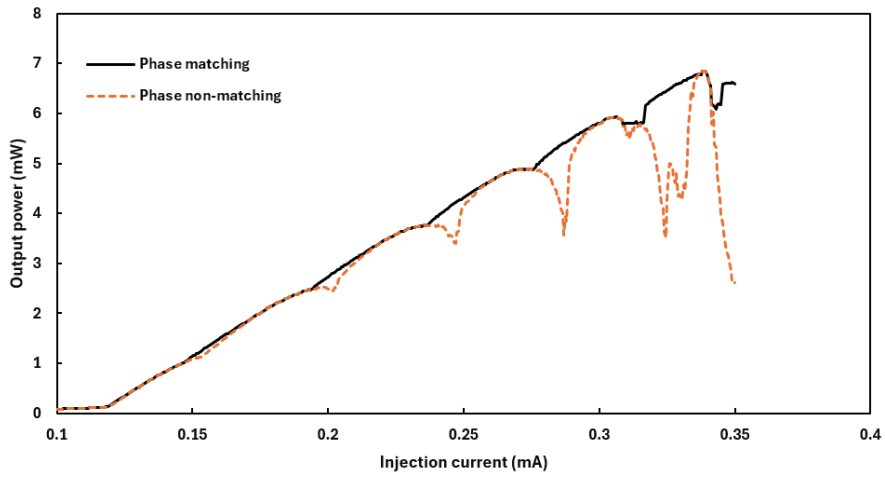

Figure 62: Assembled tunable laser IL curve measurements at room temperature. Dotted black – without tuning the phase shifter, Orange – by tuning the phase shifter and maximizing the output power.

Finally, to demonstrate full operation of the tunable laser, wavelength emission measurement with fine tuning was performed. As shown in Figure 63, the output of the assembled laser was put close to the input of a single mode fiber that is connected to an OSA.

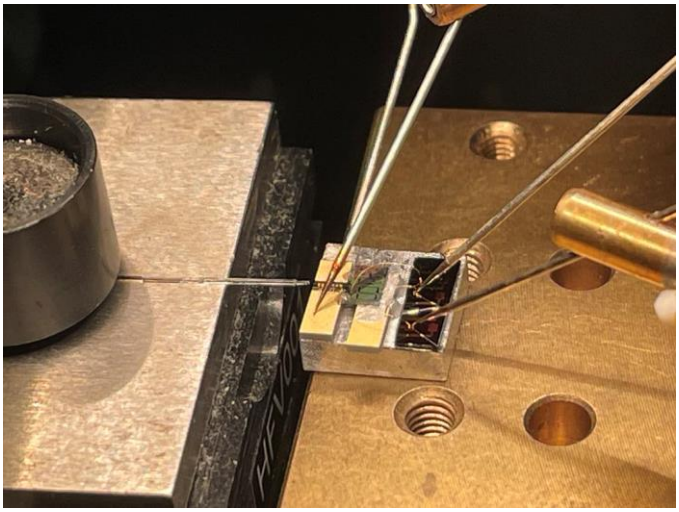

Figure 63: Lab setup to measure the wavelength emission of the assembled tunable laser

A constant current of 230 mA was injected into the RSOA to ensure the laser was stable beyond the threshold. In addition, two probes were used to apply voltage across the tuning DBRs. As shown in Figure 64, a small tuning of approximately 0.1 nm was achieved at 3 different voltages which translates to 3 different power values.

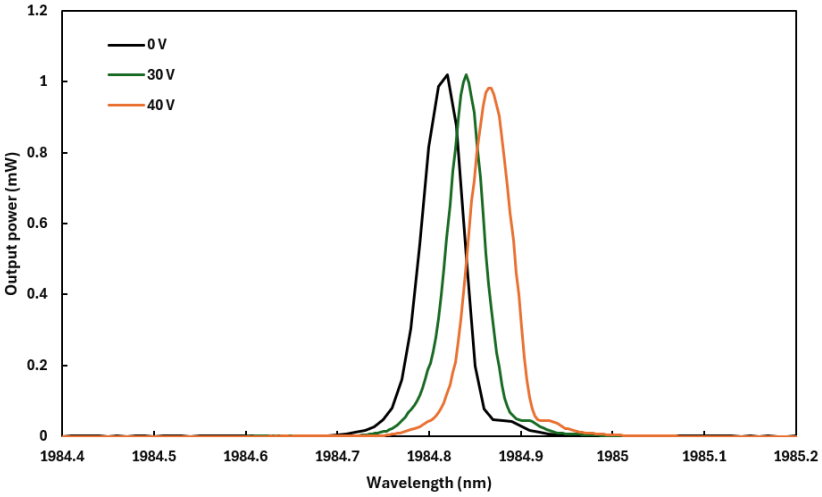

Figure 64: Wavelength tuning of the assembled tunable laser

The current through the PIC was measured at each voltage to evaluate the power needed to tune the assembled laser. The black curve corresponds to 0 V which corresponds to an input power of 0 W, while the central wavelength was recorded to be 1984.8 nm with a maximum output power of 1 mW, this introduces a shift of 7 nm to the simulated central emission wavelength of 1991.8 nm as shown in Figure 65. This shift can be attributed to the difference between the simulated refractive index and the refractive index of the fabricated device. The green curve corresponds to 30 V which corresponds to an input power of 15.9 mW, while the central wavelength is recorded to be 1984.85 nm with a maximum output power of 1 mW. Finally, the orange curve corresponds to 40 V which corresponds to an input power of 29.2 mW, while the central wavelength is recorded to be 1984.89 nm with a maximum output power of 0.97 mW. Although full tuning range measurement was not done, wavelength tuning was demonstrated after the assembly.

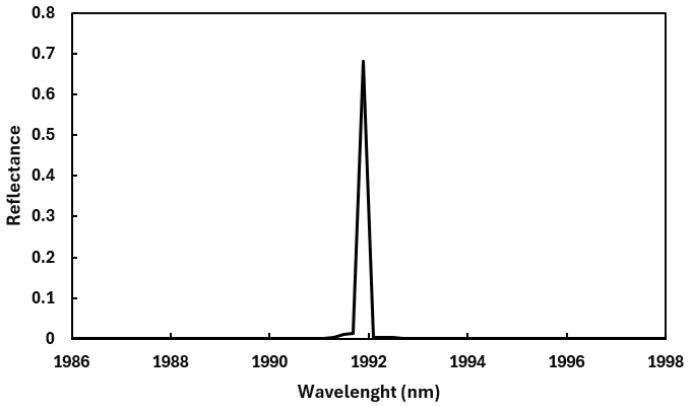

To sum up, all observations and conclusions made during the RSOA/passive WG assembly were taken into consideration during the RSOA/PIC assembly. This resulted in a successful assembly of a hybrid tunable laser. The assembled laser outperformed the same device before assembly by reaching higher power levels and lower current

threshold. Finally, wavelength tuning was demonstrated to validate the functionality of the hybrid tunable laser.

Conclusion

Semiconductor tunable lasers offer many advantages to different applications in communication, sensing, spectroscopy and medicine fields. Their miniaturization testifies for the small size, low cost, and integrability advantages. However, assembly and packaging of semiconductor tunable lasers is a complicated process with many challenges. It requires a repeatable and reliable sub-micron alignment process. Hence, any micron misalignment can lead to a degradation in the performance making the devices not robust.

In this thesis, a reliable and repeatable UV-curable adhesives assembly for hybrid tunable lasers was developed. This included a study about the important adhesive properties before the selection process. Consequently, two adhesive characterization experiments were done. The first one was to control the adhesive dispensing parameters and characterizing the dispensed volume at each pressure-application time. The second one was to find the optimum curing profile for the adhesive used in the assembly process. The assembly between the RSOA and the PIC was designed with all the components required to tackle alignment, heat dissipation, and mechanical stability challenges. Afterward, the assembly machine was programmed for a semi-automated process. Firstly, the process was validated through assembly of RSOAs and passive WGs. One of the main findings of these trials is that the used adhesive showed a continuous degradation over time due to the relaxation effect. However, this effect was taken into account while doing the assembly of the GaSb-based RSOA and the Si_3N_4 PIC. The assembled tunable laser showed a high-performance indicated in a low threshold current of 117 mA and a high maximum output power of 7.7 mW. In addition, wavelength tuning of 0.1 nm was demonstrated. These results were compared to the same device measurements before assembly in addition to the wavelength emission simulation.

Most of the objectives stated at the beginning of the thesis were realized. However, since it was a short-term project spanning 6 months, it had its own limitations. For instance, packaging the device which should have been the last step was not done as the assembled device showed degradation under the exposure of high temperatures. Hence, bonding the device into the butterfly package was not possible without thermally conductive and room-temperature curable materials. Finally, more research and experiments are needed to realize robust and reliable packaged semiconductor tunable lasers that will be ready for real-applications usage.

Future work

As stated in the conclusion, the study was time-limited and requires more experiments to realize a full packaging process of semiconductor tunable lasers. Firstly, experiments to characterize the volumetric and linear shrinkage of the adhesives are necessary to optimize the gap between the chips during the assembly. Secondly, heat-transfer simulations are to be done to assess the performance of the designed heat dissipation platforms. Thirdly, thermally conductive and room-temperature curable underfill materials need to be studied as they can tackle the gap challenge mentioned in section 2.2.1. In addition, they can be the solution for bonding the assembled device into the butterfly package. Finally, different adhesives are going to be studied to make sure that the process design is universal and can be used for different projects. For example, Optocast 3410, which has the best properties for this project, is to be purchased and tried out. The main advantage of this adhesive is its ultra-low linear shrinkage of 0.07%. Hence, shrinkage and relaxation characterization experiments are to be designed to optimize the use of this adhesive.

Bibliography

[1] R. N. Hall, G. E. Fenner, J. D. Kingsley, T. J. Soltys, and R. O. Carlson, "Coherent Light Emission From GaAs Junctions," *Phys. Rev. Lett.*, vol. 9, no. 9, pp. 366–368, Nov. 1962, doi: 10.1103/PhysRevLett.9.366.

[2] V. Heikkinen, *Tunable laser module for fibre optic communications*. in VTT publications, no. 528. Espoo: VTT, 2004.

[3] F. J. Duarte, *Tunable laser optics*, Second edition. Boca Raton: CRC Press, 2017.

[4] L. A. Coldren, S. W. Corzine, and M. Mashanovitch, *Diode lasers and photonic integrated circuits*, 2nd ed. Hoboken, N.J.: Wiley, 2012.

[5] C. Yang *et al.*, "Advances in silicon-based, integrated tunable semiconductor lasers," *Nanophotonics*, vol. 12, no. 2, pp. 197–217, Feb. 2023, doi: 10.1515/nanoph-2022-0699.

[6] Y. Ueda, Y. Saito, T. Shindo, S. Kanazawa, and M. Ishikawa, "High-speed Tunable Laser Based on Electro-optic Effect for Wavelength Switching," *NTT Technical Review*, vol. 20, no. 4, pp. 65–73, Apr. 2022, doi: 10.53829/ntr202204ra1.

[7] Y. Cunyun, *Tunable External Cavity Diode Lasers*. WORLD SCIENTIFIC, 2004. doi: 10.1142/5694.

[8] D. Liang and J. E. Bowers, "Recent progress in lasers on silicon," *Nature Photon*, vol. 4, no. 8, pp. 511–517, Aug. 2010, doi: 10.1038/nphoton.2010.167.

[9] B. G. Yacobi, S. Martin, K. Davis, A. Hudson, and M. Hubert, "Adhesive bonding in microelectronics and photonics," *Journal of Applied Physics*, vol. 91, no. 10, pp. 6227–6262, May 2002, doi: 10.1063/1.1467950.

[10] M. A. Uddin and H. P. Chan, "Adhesive technology for photonics," in *Advanced Adhesives in Electronics*, Elsevier, 2011, pp. 214–258. doi: 10.1533/9780857092892.2.214.

[11] M. Ishizaka and H. Yamazaki, "Wavelength tunable laser using silica double ring resonators," *Electron Comm Jpn Pt II*, vol. 89, no. 3, pp. 34–41, Mar. 2006, doi: 10.1002/ecjb.20212.

[12] N. Kobayashi *et al.*, "Silicon Photonic Hybrid Ring-Filter External Cavity Wavelength Tunable Lasers," *J. Lightwave Technol.*, vol. 33, no. 6, pp. 1241–1246, Mar. 2015, doi: 10.1109/JLT.2014.2385106.

[13] Y. Fan *et al.*, "Hybrid integrated InP-Si_3N_4 diode laser with a 40-Hz intrinsic linewidth," *Opt. Express*, vol. 28, no. 15, p. 21713, Jul. 2020, doi: 10.1364/OE.398906.

[14] Y. Guo *et al.*, "Thermally Tuned High-Performance III-V/Si_3N_4 External Cavity Laser," *IEEE Photonics J.*, vol. 13, no. 2, pp. 1–13, Apr. 2021, doi: 10.1109/JPHOT.2021.3068529.

[15] S. Ojanen *et al.*, "Widely Tunable (2.47–2.64 μm) Hybrid Laser Based on GaSb/GaInAsSb Quantum-Wells and a Low-Loss Si_3N_4 Photonic Integrated Circuit," *Laser & Photonics Reviews*, vol. 17, no. 7, p. 2201028, Jul. 2023, doi: 10.1002/lpor.202201028.

[16] N. Zia *et al.*, "Widely tunable 2 μm hybrid laser using GaSb semiconductor optical amplifiers and a Si_3N_4 photonics integrated reflector," *Opt. Lett.*, vol. 48, no. 5, p. 1319, Mar. 2023, doi: 10.1364/OL.480867.

[17] "CustomLine CL1500 to support integrated photonics eco-system development at ORC, Tampere University - ficonTEC," *ficonTEC*, Nov. 20, 2020. https://www.ficontec.com/customline-cl1500-to-support-integrated-photonics-eco-system-development-at-orc/

[18] "OPTOCAST 3410 - EMIUV," *EMIUV - Electronic Materials*, Aug. 31, 2021. https://emiuv.com/optocast-3410/

[19] "DELO DUALBOND ® OB786." Available: https://www.inseto.co.uk/wp-content/uploads/2023/04/DB-OB786-TDS.pdf

[20] "Technical Datasheet Vitralit ® 1860." Available: https://www.panacol.com/panacol/datasheets/vitralit/vitralit-1860-english-tds-panacol-adhesive.pdf

[21] "Technical Datasheet Norlan Optical Adhesive 61 – NOA61." Available: https://www.norlandprod.com/literature/61tds.pdf

[22] "2600B Source Measure Units (SMU) Instruments | Tektronix," Available: *www.tek.com*. https://www.tek.com/en/datasheet/2600b-source-measure-units-smu-instruments